

The Fas trimer hysteron model: bistability in apoptosis from receptor clustering

Kenneth L. Ho^{1,2} and Heather A. Harrington^{3,4}

¹Courant Institute of Mathematical Sciences, New York University, New York, NY, USA

²Program in Computational Biology, New York University, New York, NY, USA

³Department of Mathematics, Imperial College London, London, UK

⁴Centre for Integrative Systems Biology at Imperial College, Imperial College London, London, UK

Correspondence to: Kenneth L. Ho^{1,2} Courant Institute of Mathematical Sciences, New York University, 251 Mercer Street, New York, NY 10012, USA. Tel.: +1 212 998 3227; Fax: +1 212 995 4121; Email: ho@courant.nyu.edu

Abstract

Apoptosis is a highly regulated cell death mechanism involved in many physiological processes. One of the key components of extrinsically activated apoptosis is the death receptor Fas, which, on binding to its cognate ligand, oligomerize to form the death-inducing signaling complex, a pivotal trigger of apoptosis. Motivated by recent experimental data demonstrating the capacity of Fas to self-stabilize in their signaling forms, we propose a mathematical model of death ligand-receptor interaction that exhibits hysteresis. This provides an upstream mechanism for bistability in apoptosis, which is seen to be a consequence of biologically observed receptor trimerization. We analyze the bistability thresholds of the model, which furthermore possesses robustness of bistability, and provide a model assessment criterion using tools from algebraic geometry. Our results strongly suggest a role for Fas and other death receptors in generating robust threshold switching between coherent life and death states. Discussion includes an analogy with ferromagnetism and the generalization of self-stabilization to other apoptotic complexes such as the apoptosome.

Running title: Fas trimer hysteron model

Subject Categories: Simulation and data analysis / Differentiation & Death

Keywords: apoptosis / bistability / death-inducing signaling complex / hysteresis / mathematical modeling

Character count: 59,471

Introduction

Apoptosis is a coordinated cell death program employed by multicellular organisms that plays a central role in many physiological processes. Normal function of apoptosis is critical for development, tissue homeostasis, cell termination, and immune response, and its disruption is associated with pathological conditions such as developmental defects, neurodegenerative disorders, autoimmune disorders, and tumorigenesis (Fulda and Debatin, 2006; Kerr et al., 1972; Meier et al., 2000; Raff, 1998; Taylor et al., 2008; Thompson, 1995; Wyllie et al., 1980). Due to its fundamental importance, apoptosis has been the subject of intense active research,

and much has been learned of the biochemical pathways involved. Indeed, the maturity of the field has, in recent years, enabled the proliferation of mathematical models, both mechanistic and integrative, which have, in aggregate, contributed significantly to the theoretical analysis and understanding of the underlying molecular interactions (Albeck et al., 2008a,b; Bagci et al., 2006; Cui et al., 2008; Eißing et al., 2005, 2004; Fussenegger et al., 2000; Harrington et al., 2008; Hua et al., 2005, 2006; Janes et al., 2005; Lai and Jackson, 2004; Legewie et al., 2006; Nakabayashi and Sasaki, 2006; Okazaki et al., 2008; Rangamani and Sirovich, 2007; Ryu et al., 2008; Stucki and Simon, 2005). The current work takes a similarly mathematical approach and hence inherits from this legacy.

There are two main pathways of apoptotic activation: the extrinsic (receptor-mediated) pathway and the intrinsic (mitochondrial) pathway, both of which are highly regulated (Budihardjo et al., 1999; Danial and Korsmeyer, 2004). In this study, we focus on the core machinery of the extrinsic pathway, which is initiated upon detection of an extracellular death signal, e.g., FasL, a homotrimeric ligand that binds to its cognate death receptor, Fas, in a 1:3 ratio. This clusters the intracellular receptor death domains and promotes the ligation of FADD, forming the death-inducing signaling complex (DISC) (Ashkenazi and Dixit, 1998; Peter and Krammer, 1998, 2003). The DISC recruits initiator caspase zymogens, e.g., procaspase-8, through death effector domain interactions, and catalyzes their activation to, e.g., caspase-8. Initiator caspases then activate effector caspases, e.g., procaspase-3/caspase-3, which ultimately execute cell death by direct cleavage of cellular targets (Nicholson, 1999; Nicholson and Thornberry, 1997; Nuñez et al., 1998; Thornberry and Lazebnik, 1998).

Apoptosis is typically thought of as a bistable system, ideally irreversible bistable, with attracting life and death states, and a sharp all-or-none switch in between. This bistability is important for conferring biological robustness (Kitano, 2004). Consequently, researchers have used computational models to identify and study potential sources of bistability in apoptosis, including positive caspase feedback (Eißing et al., 2004), inhibition of DISC by cFLIP (Bentele et al., 2004), cooperativity in apoptosome formation (Bagci et al., 2006), double-negative caspase feedback through XIAP (Legewie et al., 2006), and double-negative feedback in Bcl-2 protein interactions (Cui et al., 2008). In this work, we propose that bistability may be induced upstream by the death receptors themselves.

The current model of death ligand-receptor dynamics supposes that FasL recruits Fas independently at each of three binding sites, thereby producing a steady-state DISC concentration that varies smoothly with the input ligand concentration (Harrington et al., 2008; Lai and Jackson, 2004). However, recent structural data by Scott et al. (2009) suggests a different view. Briefly, Fas was found to exist in both closed and open forms, only the latter of which allows FADD binding and hence transduction of the apoptotic signal. Moreover, open Fas were shown to be capable of self-stabilization through stem helix and globular interactions. This immediately affords a mechanism for bistability, much akin to the celebrated Ising model in ferromagnetism (Ising, 1925), in which open Fas, disfavored relative to their native closed forms, are able to sustain their conformations even after removal of the initial stimulus promoting receptor opening, past a certain critical density of open Fas. This induces hysteretic behavior in the concentration of active, signaling receptors and therefore in apoptosis. The Fas trimer hysteron model is a mathematical formulation of this idea, which furthermore provides a possible rationale for the observed 1:3 binding stoichiometry. The essential interpretation is that FasL acts as a clustering platform for Fas (Figure 1A), which then establish contacts through pairwise and higher-order interactions to form units capable of hysteresis, i.e., hystérons.

Results

Model formulation and bistability

The bistable character of the hysteron model is contingent on the necessity of receptor clustering by FasL for high-order Fas interactions. Thus, we proceeded first with a simple estimate of Fas density in the membrane.

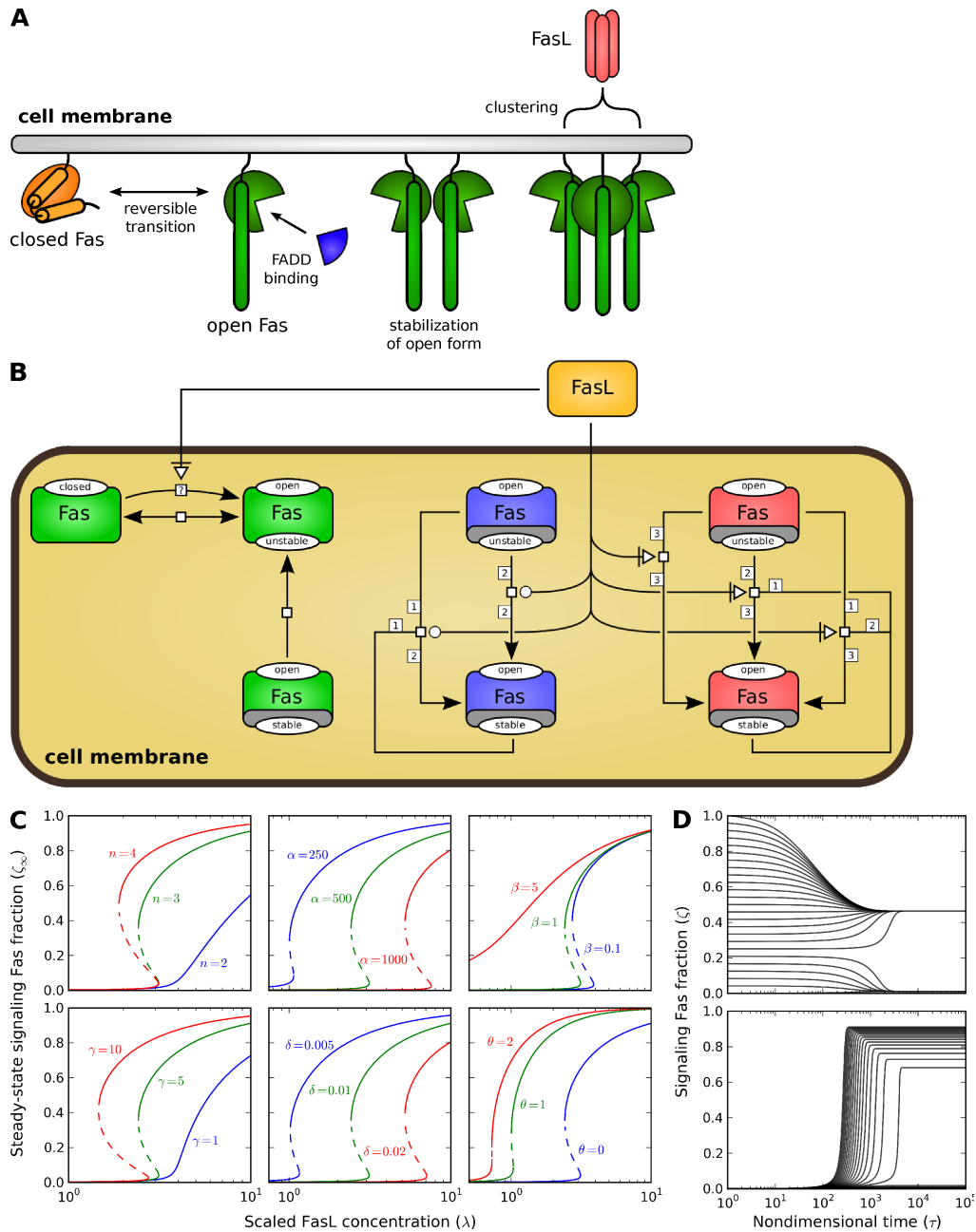


Figure 1 The Fas trimer hysteron model. All parameters were set at baseline values (Table I) unless otherwise stated. (A) The transmembrane death receptor Fas natively adopts a closed conformation, but can open to allow the binding of FADD, an adaptor molecule that facilitates apoptotic signal transduction. Open Fas can self-stabilize via stem helix and globular interactions, which may be enhanced by receptor clustering through association with the ligand FasL. (B) Process diagram (SBGN PD L1) of the hysteron model with $n = 3$ (Box 1). Fas exists in three forms: closed; open, unstable; and open, stable. Green entities are capable of ligand-independent processes, where we have marked ligand-induced receptor opening as uncertain; blue, ligand-catalyzed processes of molecularity two; and red, ligand-necessary processes of molecularity three. (C) Variational effects of model parameters on the steady-state signaling Fas fraction ζ_∞ as a function of the scaled FasL concentration λ . Full and dashed lines indicate stable and unstable steady states, respectively. Bistability requires $n \geq 3$ ($n = 3$ for receptor trimerization). (D) Time courses at baseline parameters for λ fixed within the bistable regime and variable ζ^0 , the initial signaling Fas fraction (top); and fixed ζ^0 and variable λ (bottom).

Table I Baseline nondimensional parameter values for the hysteron, crosslinking, and caspase models.

Model	Parameter	Value
hysteron	n	3
	α	500
	β	1
	γ	5
	δ	0.01
	θ	0
crosslinking	κ	0.1
caspase	π_ϕ	10
	π_ψ	10
	π_δ	1
	σ	0.1

Previous models incorporating ligand-receptor dynamics have all used Fas concentrations on the order of 10–100 nM (Albeck et al., 2008a,b; Bentele et al., 2004; Harrington et al., 2008; Hua et al., 2005; Okazaki et al., 2008), so conservatively taking an estimate of 100 nM gives an areal density of $\sim 10^{-4}$ molecules/nm². We hence found that receptors are sparsely distributed, with only about one Fas molecule in the area accessible around each receptor, assuming a characteristic size of 100 nm. High-order Fas interactions (i.e., termolecular and above) in the absence of FasL were therefore neglected.

The model includes constitutive receptor opening and closing, pairwise open Fas stabilization, higher-order open Fas stabilization enabled by FasL, and ligand-induced receptor opening (Figure 1B). For simplicity, mass action was used to describe the chemical kinetics. The resulting model has three receptor species, five reaction forms, and, at steady state, is characterized by seven nondimensional parameters (Box 1). The steady state is given by solving a polynomial equation of degree n , denoting the number of receptors that each ligand can coordinate, which, significantly, admits bistability only if $n \geq 3$. In the context of this model, the biologically observed value of $n = 3$ thus demonstrates the lowest-order complexity required for bistability. The model was shown to indeed exhibit bistability (Figure 1C and D) for reasonable parameter choices (see Table I). Notably, the bistability is reversible, as the governing polynomial reduces to a quadratic in the absence of ligand; alternatively, from a dynamical systems perspective, the steady-state structure undergoes a saddle-node bifurcation as FasL is decreased.

For the remainder of this study, we restricted to the biological case of $n = 3$. Moreover, intuition suggests that ligand-induced receptor opening is not crucial for bistability, hence for simplicity, we further set $\theta = 0$, with the understanding that the error so incurred is only cursory at this level and thus unlikely to change the essential character of the following results.

Bistability thresholds and robustness

Having established the capacity of the model for bistability, we then sought to study its defining features in more detail by using a combination of analytical and numerical tools. In particular, we focused on the activation and deactivation thresholds λ_\pm , respectively, that define the bistable regime; these are the points at which the steady state switches discontinuously from one branch to the other, and are given by the values of λ at which the hysteresis curve turns, i.e., at $\partial\lambda/\partial\zeta_\infty = 0$ (Figure 2A). These critical values of λ imply a polynomial equation in ζ_∞ of order four, which, through an asymptotic analysis with $\alpha = \mathcal{O}(1/\varepsilon)$,

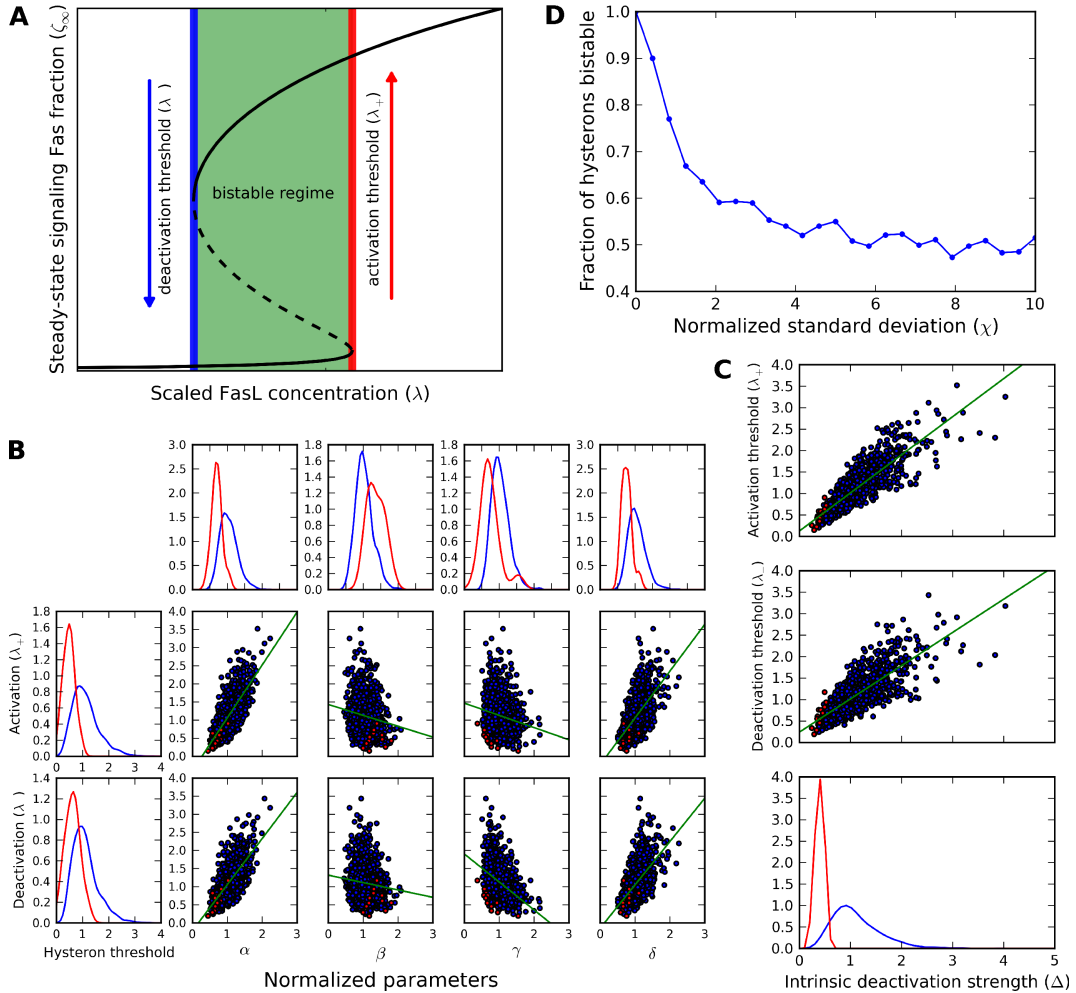


Figure 2 Bistability thresholds and robustness. **(A)** Definition of the activation and deactivation thresholds λ_{\pm} , which bound the bistable regime of the model. **(B)** Parameter and threshold variation for $N = 10^3$ samples (Dataset 1), where the parameters α , β , γ , and δ were drawn independently from log-normal distributions with scaled standard deviation $\chi = 0.25$ about baseline median values (Table 1). Parameters are expressed relative to their baseline values, and thresholds relative to their values at baseline parameters. Scatter plots reveal relationships between the parameters and their induced thresholds (green, linear regressions), and marginal probability distributions (top, parameters; side, thresholds) characterize the total variation of each quantity. For both visualizations, blue corresponds to samples with bistability, and red to those without. **(C)** Threshold variation with the intrinsic deactivation strength Δ (data and visualization as in B). **(D)** Robustness of bistability. Data were generated over $0 \leq \chi \leq 10$ (N samples each; protocol as in B), and the fraction of bistable samples recorded (Dataset 2). The bistable proportion remains substantial at ≈ 0.5 even under extreme variation.

$\beta, \gamma = \mathcal{O}(1)$, and $\delta = \mathcal{O}(\varepsilon)$ for $\varepsilon \ll 1$, we showed to have at most two nonnegative roots, namely

$$\zeta_+ \sim \sqrt{\frac{2\Delta}{\alpha[\gamma(\Delta-1) - \Delta]}}, \quad (1)$$

$$\zeta_- \sim \sqrt{\frac{\Delta\Theta}{\gamma}} - (\Delta-1), \quad (2)$$

where

$$\Delta = \frac{\alpha\delta}{\beta}, \quad (3)$$

$$\Theta = \gamma(\Delta-1) - 1, \quad (4)$$

with the consistency requirement that $\zeta_+ = \mathcal{O}(\sqrt{\varepsilon})$ and $\zeta_- = \mathcal{O}(1)$ (Supplementary Note 1). These correspond to

$$\lambda_+ \sim \beta(\Delta-1), \quad (5)$$

$$\lambda_- \sim \frac{\beta}{\gamma\Delta + \Theta - 2\sqrt{\gamma\Delta\Theta}}, \quad (6)$$

respectively, which are both of $\mathcal{O}(1)$. This fully characterizes the bistability in the asymptotic limit (Supplementary Figure 1). Note that α and δ only enter these expressions together through Δ ; this likely explains their similar variational effects (Figure 1C).

The asymptotic forms of the thresholds reveal their critical dependence on Δ , the relative intrinsic deactivation strength. In particular, provided that $\gamma > 1$, all thresholds are real and nonnegative if

$$\Delta > \Delta^* \equiv \max\left\{\frac{\gamma}{\gamma-1}, \frac{\gamma+1}{\gamma}\right\} > 1. \quad (7)$$

We hence assumed that $\gamma > 1$, which quantifies the intuition that ligand-enabled higher-order receptor cluster-stabilization is favored over the corresponding pairwise stabilization, as due to, e.g., aggregate globular interactions. Thus, given the well-ordering of the ζ_{\pm} , the asymptotic bistability condition is $\Delta > \Delta^*$. Robustness of bistability is therefore immediate if $\Delta \gg \Delta^*$ at baseline values; in this regime, we expect the model to retain sharp switching behavior, and hence a robust distinction between coherent life and death states, over a wide operating range.

To study the bistability thresholds in general, we turned to numerical computation. Parameters were drawn independently from log-normal distributions with scaled standard deviations of $\chi = 0.25$ relative to baseline median values (Table I and Supplementary Table II; Dataset 1). The resulting thresholds are not particularly robust, exhibiting variations of $\chi(\lambda_{\pm}) \approx 0.5$. However, robustness to specific parameters was observed, notably both λ_{\pm} to β , and λ_+ additionally to γ (Figure 2B and Supplementary Table III).

Almost 99% of parameter sets were bistable, despite significant variation in the parameters and corresponding thresholds. Thus, the model exhibits robustness of bistability. While none of the natural system parameters provided effective discrimination for bistability, consistent with the analysis, we found that the simplified condition $\Delta > 1$ accurately characterizes the data, correctly classifying over 98% of parameter sets (Figure 2C). Our baseline parameters give $\Delta = 5$, so the expected robustness is substantial, as observed. A simple argument further suggests that, given $\gamma > 1$, this robustness asymptotes toward 50% bistability as $\chi \rightarrow \infty$ (Supplementary Table IV). Parameters sampled widely over $0 \leq \chi \leq 10$ support this (Figure 2D and Dataset 2).

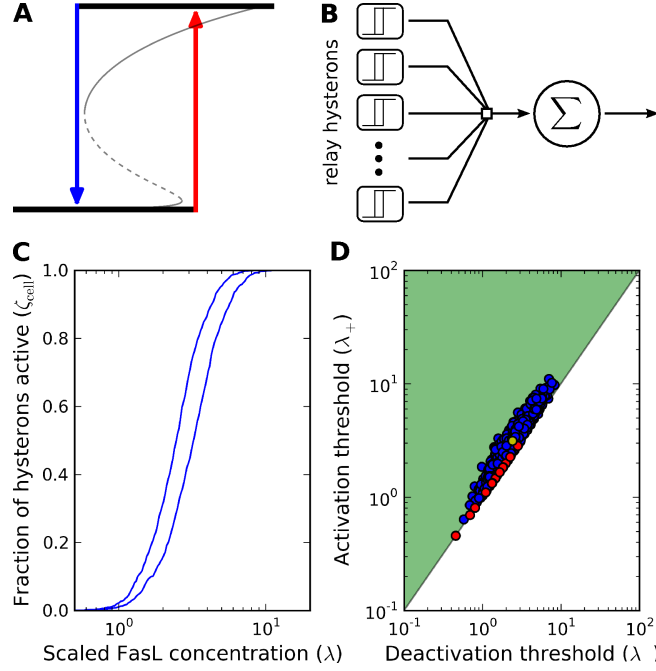


Figure 3 Cell-level analysis using relay hysterons. **(A)** Digital abstraction as a relay hysteron, defined as either *active* or *inactive*, corresponding to high Fas signaling, respectively (thick black lines). State switching occurs according to the activation and deactivation thresholds (red and blue arrows, respectively) and the local FasL concentration. **(B)** Schematic diagram of the Preisach model. The activities of an ensemble of independent relay hysterons are summed to give the total output activity; in our case, due to normalization, the total activity is an average. **(C)** and **(D)** Cell analysis using Preisach averaging on relay hysterons defined on the threshold variation data (Dataset 1). **(C)** Hysteresis curve of cell activity ζ_{cell} . **(D)** Distribution of thresholds on the Preisach plane (green); coloring as in Figure 2B and C, where additionally, the thresholds at baseline parameters (Table I) are shown in yellow.

Cell-level analysis using relay hysterons

The model thus far has been formulated based on constant parameters. At the level of the cell, however, this is unlikely to be true due to local inhomogeneities, e.g., variations in receptor concentration, lipid composition, and other membrane factors, as well as to stochasticity at low molecule numbers (see Supplementary Note 3). These issues may be treated simultaneously by applying the model locally within some membrane patch—i.e., by dividing the cell into individual hysteretic units—and positing the cell as an array of such hysterons, each with parameters drawn randomly from an appropriate distribution. For ease of analysis, we further applied a digital abstraction, whereby each hysteron is either *active* or *inactive*, depending on the local ligand concentration and its activation and deactivation thresholds. More precisely, the abstracted activity of a given hysteron is

$$\hat{\zeta} = \begin{cases} 0, & \lambda \leq \lambda_-, \\ 1, & \lambda \geq \lambda_+, \\ \hat{\zeta}_0, & \lambda_- < \lambda < \lambda_+, \end{cases} \quad (8)$$

where $\hat{\zeta}_0$ is its previous activity level and hence accounts for its memory (Figure 3A). Thus, the cell is viewed

as a set of relay hysterons connected in parallel, whose sum activity gives the total (normalized) cell response

$$\zeta_{\text{cell}} = \frac{1}{N} \sum_{i=1}^N \hat{\zeta}_i, \quad (9)$$

where $\hat{\zeta}_i$ is the activity of hysteron i (Figure 3B). Observe that this is simply the classical Preisach model (Preisach, 1935), which has enjoyed remarkable success in describing magnetic hysteresis (Barker et al., 1983).

We used the data previously generated at $\chi = 0.25$ (Dataset 1) to trace out a cell-level hysteresis curve under the assumption of a uniform ligand distribution (Figure 3C). Clearly, this is a smoothing operator, averaging over the sudden shifts associated with each hysteron. Indeed, this idea has been applied previously to explain experimentally measured population-level data: by summing over individual hysteretic cells, sharp thresholds are smeared out, producing a smooth, graded population response (Eiřing et al., 2004). Note, though, that the current analysis predicts a graded response at the cell level; whether this is true remains as yet beyond the reach of experiment. Moreover, the lack of a sharp switch from low to high Fas signaling does not necessarily imply the same at the level of the caspases which ultimately govern cell death, as downstream components may possess switching dynamics (see, e.g., Bagci et al., 2006; Bentele et al., 2004; Cui et al., 2008; Eiřing et al., 2004; Legewie et al., 2006). In principle, the bistability thresholds may be distributed randomly on the Preisach plane, but we in fact observed a strong linear dependence between the λ_{\pm} ($r > 0.95$; Figure 3D). This suggests an intrinsic ordering of the thresholds that promotes bistability and hence robustness.

Comparison with the crosslinking model

The prevailing model of ligand-receptor interaction in apoptosis is based on a crosslinking formulation, whereby FasL recruits Fas independently at each of three binding sites. As a representative of such models, we analyzed a variant of that by Lai and Jackson (2004), as introduced in Harrington et al. (2008); other formulations include Hua et al. (2005) and, for more simplified versions, see Albeck et al. (2008a,b); Bentele et al. (2004); Fussenegger et al. (2000).

The crosslinking model describes reversible binding at each site and admits only one steady state (Box 2 and Figure 4A). In analogy with the hysteron model, we used

$$\zeta \equiv \gamma_1 + 2\gamma_2 + 3\gamma_3 = 1 - \rho \quad (10)$$

as a measure of the signaling Fas fraction (Figure 4B). Clearly, the crosslinking model cannot be bistable, in contrast to the hysteron model. In principle, therefore, this provides a ready criterion for model discrimination, assuming that the ligand-receptor dynamics can be isolated. Alternatively, if this level of experimental control cannot be exercised, we provide also a discrimination test based on steady-state invariants derived using tools from algebraic geometry, following Manrai and Gunawardena (2008). The basic idea is that dynamics resulting from mass action chemical kinetics are polynomial equations in the species concentrations; consequently, their steady states describe algebraic curves, whose intersection—describing the steady states of the system—is an algebraic variety that can be studied using algebraic geometry.

Our primary tool is the Gröbner basis, which we used to compute steady-state invariants of each model, i.e., polynomials in the species concentrations that vanish at steady state (Box 3), with respect to the observables λ_0 , the total FasL concentration, presumably a controlled experimental input; and ζ , the active Fas concentration, which may be measured, for example, by using FADD binding as an indicator. The identification of experimental observables is important as concentrations that cannot be measured must, in principle, remain unknown and hence be eliminated from any experimentally relevant invariant. Gröbner bases readily allow such elimination to be performed. With each system expressed in terms of λ_0 and ζ ,

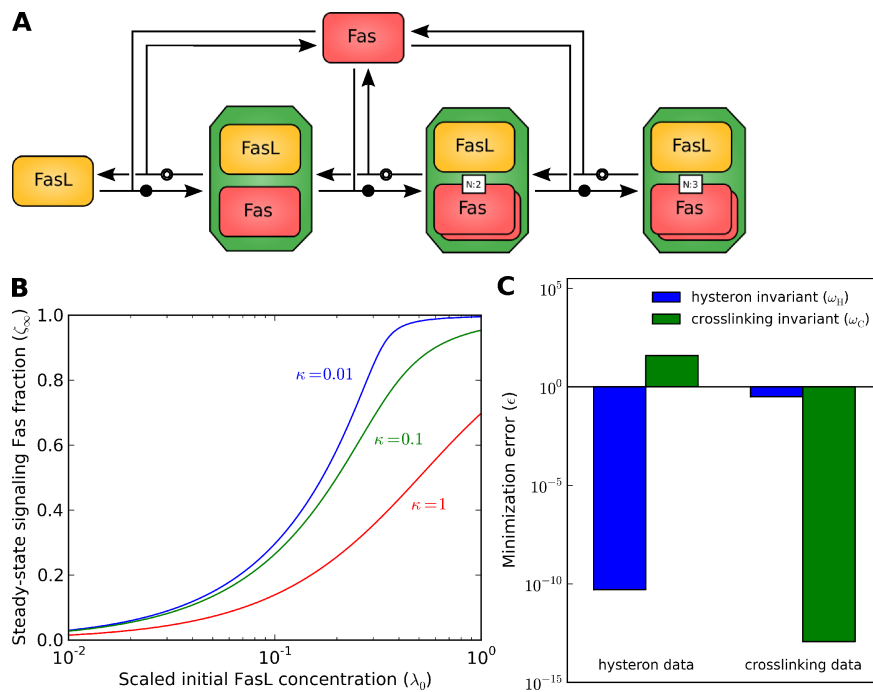


Figure 4 Comparison with the crosslinking model. (A) Process diagram (SBGN PD L1) of the crosslinking model (Box 2). (B) Variation of the steady-state signaling Fas fraction ζ_∞ with respect to the model parameter κ . (C) Minimization errors ϵ of the steady-state invariants ω_H and ω_C for the hysteron and crosslinking models, respectively (Box 3), over data generated from each model (Datasets 3 and 4) using nonnegative least squares (see Materials and methods for details).

and all other variables eliminated, the resulting steady-state invariants ω_H and ω_C for the hysteron and crosslinking models, respectively, are polynomials of the form $\sum_{i,j} c_{ij} \lambda_0^i \zeta^j$ (Supplementary Note 4).

We may use these invariants for model discrimination by comparing the errors $\epsilon_H = |\omega_H|$ and $\epsilon_C = |\omega_C|$ for the hysteron and crosslinking models, respectively, given experimental data $(\lambda_0, \zeta_\infty)$. If the model parameters are unknown, then we may minimize ϵ_H and ϵ_C over the space of respective parameters and compare their optimal values. As a demonstration that such discrimination is feasible, we generated sample steady-state concentrations from each model (Datasets 3 and 4) and minimized the data with respect to each invariant. The problem is highly nonlinear, so to improve the optimization, we considered each term $\lambda_0^i \zeta^j$ as an independent variable, thus effectively linearizing the problem with respect to the associated coefficients c_{ij} . We further constrained the c_{ij} and hence, by relabeling, cast the minimization as a nonnegative least squares problem, which can be solved exactly in that the error achieved is a global minimum (Lawson and Hanson, 1995). The results show that the errors are small if the models underlying the data generation and the invariant minimization are the same, and large otherwise (Figure 4C). This is precisely the condition necessary for effective model discrimination.

Feedforward caspase bistability

Bistability is often taken as a required property of apoptosis, under the intuitive reasoning that a cell must possess both stable life and death states. One common way of achieving bistability is by using positive feedback; in fact, positive feedback between caspases-8 and -3, e.g., through caspase-6 (Cowling and Downward, 2002; Slee et al., 1999), has been shown to mediate bistability in the extrinsic pathway (Eißing et al., 2004). However, whether this feedback is relevant appears controversial, due, first, to its omission in several recent models (Bentele et al., 2004; Hua et al., 2005; Okazaki et al., 2008); and second, to the prediction that it does not contribute significantly to the qualitative dynamics of the system (Albeck et al., 2008b). While numerous apoptotic processes generating bistability have been identified in the intrinsic pathway (Bagci et al., 2006; Cui et al., 2008; Legewie et al., 2006), such mechanisms operating independently of caspase feedback in the extrinsic pathway are scarce, including, so far, only direct inhibition of DISC by cFLIP (Bentele et al., 2004). It is immediate, however, that the proposed hysteron model offers another solution by moving the burden of bistability from the caspases to the upstream death receptors; the model therefore provides a welcome resolution to the problem of bistability in feedforward extrinsic caspase networks.

To demonstrate this, we constructed a rudimentary feedforward model of caspase activation capturing only the most basic interactions, particularly the activation of caspase-3 by caspase-8, which itself is activated by DISC (Figure 5A). Significantly, the model has only one steady state, so in the absence of bistability at the DISC, hysteresis is clearly not possible (Box 4 and Figure 5B). To probe this directly, we coupled the model to the upstream hysteron and crosslinking models by using active Fas as a functional surrogate for DISC (Figure 5C). The results confirm that only the hysteron-caspase model achieves hysteresis (Figure 5D). The hysteron model thus provides a possible mechanism for extrinsic apoptosis to function as a bistable switch even in cells with nonexistent or weak caspase feedback.

Discussion

Summary and biological significance

In this work, we have presented a model of death ligand-receptor interaction incorporating recent experimental findings (Scott et al., 2009) that demonstrates its capacity for bistability in extrinsic apoptosis. The Fas trimer hysteron model is a mathematical formulation of the observation that Fas can aggregate and self-stabilize in their active signaling forms; in this interpretation, FasL provides a clustering platform for Fas, promoting receptor activation and hence apoptosis by enabling proximity-induced receptor interactions.

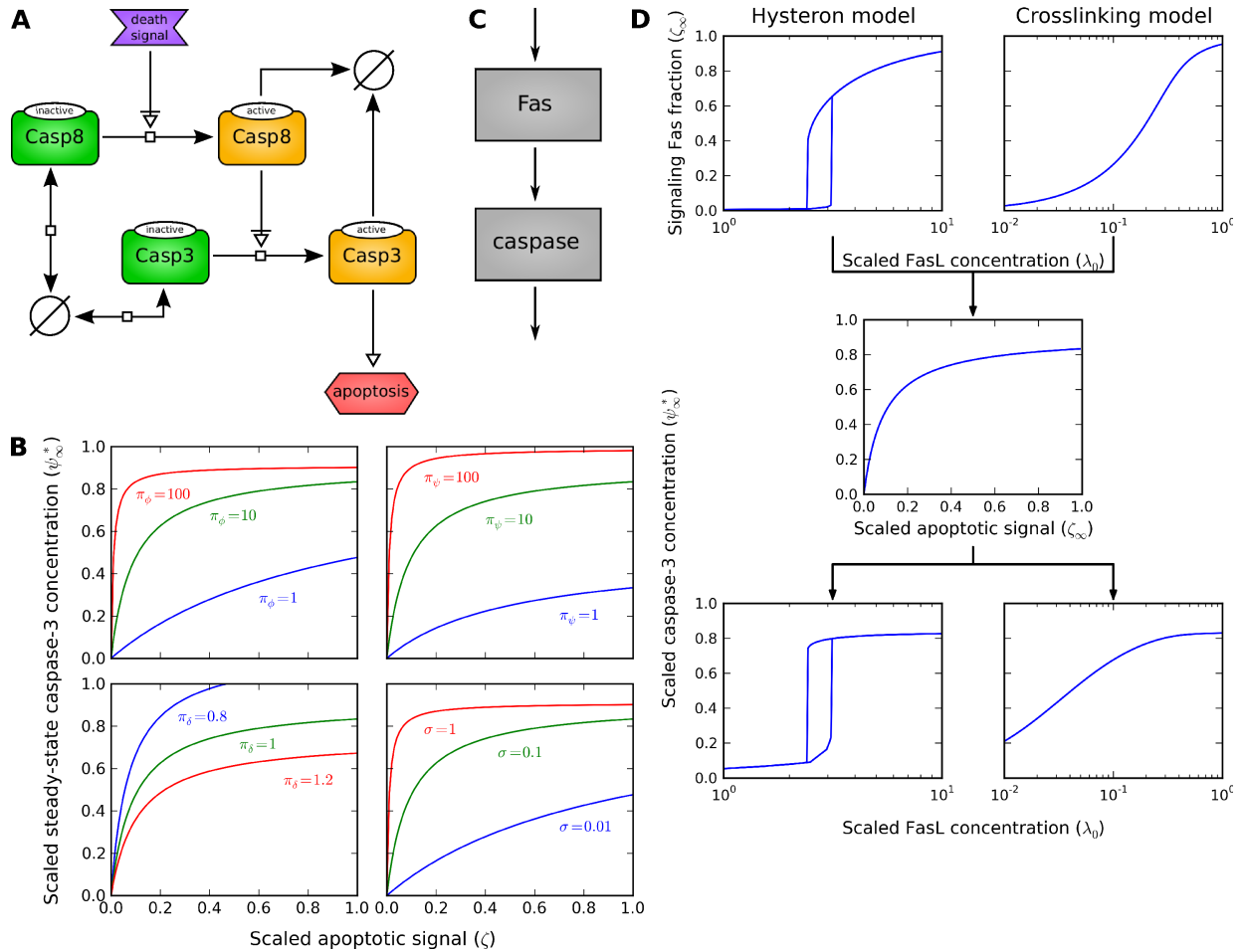


Figure 5 Feedforward caspase bistability. All parameters were set at baseline values (Table I) unless otherwise stated. (A) Process diagram (SBGN PD L1) of the feedforward caspase model (Box 4). Caspases-8 and -3 represent all initiator and effector caspases, respectively, and can each be active (orange) or inactive (green; procaspases-8 and -3, respectively). The system input is a death signal (purple; e.g., DISC or active Fas) and its output, the degree of apoptotic activation (red, taken as the caspase-3 concentration). (B) Variation of the steady-state caspase-3 concentration ψ_{∞}^* with respect to the model parameters as a function of the scaled apoptotic signal ζ . (C) Systems diagram of Fas-caspase coupling. The apoptotic signal generated by the Fas module (e.g., hysteron or crosslinking) is used as input to the downstream caspase module. (D) Hysteresis curves of caspase-coupled models using either the hysteron (left) or crosslinking (right) models for the Fas subsystem. Flow of information as in C. In the absence of caspase feedback, only the hysteron model provides a mechanism for bistability.

Although the precise mechanism by which this may occur is unclear—it is necessary only that we have captured its basic qualitative behavior—the model strongly suggests a role for Fas in generating apoptotic hysteresis, which is essential for the maintenance of an unambiguous transition between robust life and death states. Significantly, the model predicts that bistability is a consequence of receptor trimerization, which hence provides an explanation for the homotrimeric character of FasL.

The hysteron model thus implies an additional all-or-none switch in apoptosis, supplementing those that have been studied previously (Bagci et al., 2006; Bentele et al., 2004; Cui et al., 2008; Eißing et al., 2004; Legewie et al., 2006). Critically, the proposed mechanism is triggered upstream at the very death receptors that initially detect the death signal encoded by FasL; therefore, this switch is apical in that it precedes and hence provides context for all other switches in the system. Consequently, it thus operates independently of all intracellular components and so offers a general mechanism for bistability, even in cell lines deficient in, for example, caspase feedback (see Albeck et al., 2008b). As the signal received by all downstream components is hence convolved with the signature of Fas activation, we highlight the importance of understanding the mechanism and kinetics of death ligand-receptor interaction. More generally, this provides encouragement for further research into the formation of the DISC, which, in this view, may be considered the macromolecular aggregates of active Fas.

We remark that the hysteron model does not restrict only to Fas, but may apply also to related death receptors such as those in the tumor necrosis factor receptor (TNFR) family, provided that they similarly possess an active form which is capable of aggregate self-stabilization.

Model assumptions and analysis

In formulating the hysteron model, we have sought to emphasize simplicity and tractability, though often at the expense of biological realism. For instance, it is more appropriate to use Michaelis-Menten kinetics with generalized loads for all ligand-dependent reactions; however, it is clear that this should not change the essential character of the model as no new physical steady state can be introduced. Although the emergence of a new phenotype in which apoptosis cannot occur due to saturation of reaction rates is possible, this is not of practical novelty as, within the biological regime $\lambda \sim 1$ of interest, it is essentially equivalent to a mass-action hysteron with activation threshold $\lambda_+ \gg 1$.

The model invokes the assumption that higher-order Fas interactions are not permitted in the absence of FasL. This is a strong statement and should be replaced by the requirement only that any such interaction, characterized by the analogous parameter $\tilde{\gamma}$, is weak, i.e., $\tilde{\gamma} \ll 1$. But clearly this relaxation poses no difficulty, since by rescaling we see that this modification has an effect only if $\tilde{\gamma} \sim \gamma\lambda_+ = \mathcal{O}(1)$. In particular, this also shows that irreversible bistability cannot be achieved in this way.

Although we have assumed monomeric Fas, the model is not strictly incompatible with pre-ligand receptor assembly, in which Fas dimerizes or trimerizes prior to ligand exposure (Chan, 2007; Chan et al., 2000; Siegel et al., 2000). Indeed, it is necessary only that pre-associated Fas be inactive with respect to signaling via FADD binding, and furthermore be incapable of ligand-independent cluster-activation. We may then essentially apply our model locally to the region about each pre-assembled receptor complex, with the result that bistability is yet achieved. The interpretation now is that FasL acts on pre-associated Fas to induce a structural shift from a metastable pre-assembled conformation to a preferred state of aggregate activation. Notably, conformational change of the pre-assembled complex upon ligand binding has been confirmed experimentally (Chan et al., 2001); this is furthermore consistent with the finding that receptor pre-assembly promotes sensitivity to apoptosis, presumably by increasing the local receptor concentration (Muppidi and Siegel, 2004).

We have presently only considered the asymptotic limit $\alpha \gg 1$ and $\delta \ll 1$. In the event that this does not reflect reality, however, our analysis should be viewed only as a representative application of asymptotics in general, which, in this particular case, revealed the criticality of the derived parameter Δ , whose importance

would likely have eluded standard numerical sensitivity tests operating on the explicit system parameters. The value of such mathematical treatment is thus apparent. Moreover, we note that asymptotic analysis is an effective tool for biology in general, particularly for model reduction, as biological systems often contain multiple timescales that separate naturally.

Tools for model selection

A primary goal of systems biology is to construct quantitative models of biochemical processes that are mechanistically correct. However, for any given process, a number of descriptions may exist—as due to, e.g., a lack of specificity from unresolved experimental data—of which only one can in principle be correct. Model selection is therefore essential; and a scalable unbiased algorithm for doing so, particularly desirable (see, e.g., Apgar et al., 2008).

In discriminating the hysteron and crosslinking models, we used Gröbner basis methods to compute steady-state invariants, whose satisfiability can assess model correctness. This approach possesses three significant advantages: first, model parameters can be absorbed into the coefficient field over which the dynamics are described, resulting in invariants that are valid for all parameter choices and thus parameter-free selection criteria; second, experimentally relevant invariants can be generated through the elimination of variables that cannot be measured; and third, application of the method requires no sophisticated experimental control, e.g., gene knockdowns or knockouts, revealing only natural relations between the system variables. This last point deserves particular emphasis: steady-state invariants can be applied passively, tailored to the data at hand—which, for example, may be existing data—and hence present a flexible, cost-effective basis for model selection. We note furthermore that although we have so far treated only mass-action systems, the described approach can be generalized for other types of kinetics by using different fields; in fact, the current choice of $\mathbb{Z}(\mathbf{a})$ is appropriate for Michaelis-Menten and Hill reaction forms, as well as their integral polynomial generalizations.

Invariant assessment may be performed in a number of different ways. For example, Manrai and Gunawardena (2008) exploited the low effective dimensionality of invariants in multisite phosphorylation to derive a discrimination criterion based on the visual assessment of planarity. In the current work, this was not feasible, so we turned instead to numerical optimization, ultimately using nonnegative least squares (NNLS) for performance. It is profitable to remember that an invariant is simply a polynomial that vanishes, so a wide variety of methods may be well used for its analysis. For large systems, however, the method of choice will likely be optimization, and, in such cases, we feel that NNLS is a particularly strong tool: assuming effective linearization by introducing additional degrees of freedom, NNLS provides an efficient scheme for minimizing the resulting linear form exactly subject to physical constraints (Lawson and Hanson, 1995). Thus, steady-state invariants and NNLS seem to form the basis for an effective procedure for model selection and, more generally, model assessment. Scaling this up, however, is difficult, owing primarily to the bottleneck of computing Gröbner bases for large systems, though this may be overcome by embracing parallelism (Neun and Melenk, 1992) or by implementing more sophisticated algorithms such as Faugère’s F_4 and F_5 (Faugère, 1999, 2002). With such enhancements in place, a large-scale automated model assessment tool may well be achievable.

Broadly, algebraic geometry is concerned with the solutions of systems of polynomial equations. Given its generality, we hence expect algebraic geometry to find wide application across all of biology, not limited only to steady-state model characterization; for an application of Gröbner basis methods in membrane biophysics, see Faugère et al. (2003).

Alternative mechanisms for bistability

The experimental data by Scott et al. (2009) motivating this work do not constrain to the particular form of the model presented, but in fact admit a class of models operating on the basic principle of aggregate self-

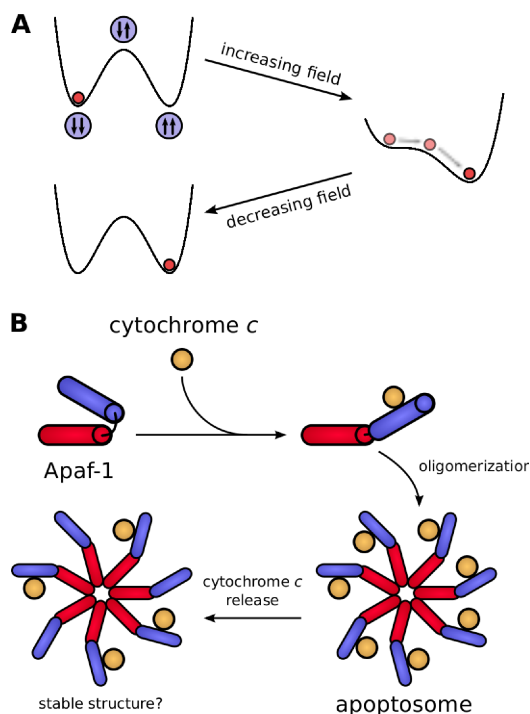


Figure 6 Alternative mechanisms for bistability. (A) Analogy with the Ising model from ferromagnetism. A mixed receptor state ($\uparrow\downarrow$) is disfavored relative to both the uniformly closed ($\downarrow\downarrow$) and open ($\uparrow\uparrow$) states, as characterized by the given potential. Introduction of ligand corresponds to the addition of an external field, which biases the potential and induces a state transition (red circle). (B) Hypothesis for bistability in apoptosome formation. Binding of cytochrome *c* to natively closed Apaf-1 produces an open conformation required for the assembly of the apoptosome, a macromolecule composed of seven Apaf-1 subunits. Considerations of symmetry and steric constraints suggest that the apoptosome is highly stable, such that its structure may persist even upon dissociation of cytochrome *c*.

stabilization, all possessing the capacity for bistability. The current form has been chosen for its simplicity and its direct illustration of why the 1:3 ligand-receptor binding stoichiometry might have evolved; this, however, is not strictly necessary, so the hysteron model may be better viewed as a representative instance of all such models, which furthermore provides a formal demonstration that the data are compatible with bistability and hysteresis—this, in truth, is the main point of this work. Nevertheless, this does not imply that the analyses performed are not generally meaningful as the resulting derived parameters certainly have general analogues, which likely play similar roles in their respective contexts in deciding bistability.

The concept of self-stabilization may be applied more intuitively by adhering to the form of the Ising model (Ising, 1925). Thus, identify open and closed receptors with up (\uparrow) and down (\downarrow) spins, respectively, and assume a local energy function that penalizes opposite neighboring spins; this is reasonable, for example, because the state $\uparrow\downarrow$ is disfavored relative to either $\uparrow\uparrow$ or $\downarrow\downarrow$ as it cannot invoke self-stabilization and additionally has to pay the price of having an open receptor. Addition of ligand corresponds to an increased propensity for receptors to open and therefore, in this model, to an external magnetic field providing a bias for up spins. A simple argument then shows that bistability is a natural consequence, which we may even make effectively irreversible by controlling the relative state energies (Figure 6A). Note, though, in this view that there appears to be nothing particularly special about the choice that receptors interact as trimers;

bistability may well be achievable for interactions of two, or four, or more units.

Interestingly, it is precisely this degeneracy that allows the notion of cluster-stabilization to apply more generally than has presently been considered. As an example, we turn to the apoptosome, a wheel-shaped caspase-activating complex in the intrinsic pathway formed by the heptamerization of Apaf-1 (Cain et al., 2002; Riedl and Salvesen, 2007; Yu et al., 2005). Similarly to Fas, Apaf-1 natively adopts a closed form, opening only upon binding of cytochrome *c*, which represents an intracellular death signal (Fumarola and Guidotti, 2004). This conformational change allows Apaf-1 to oligomerize to form the apoptosome. Presumably, the tight interlocking of Apaf-1 results in a highly stable structure, such that if cytochrome *c* were now to dissociate, it is conceivable that the apoptosome might remain intact, thus resulting in bistability (Figure 6B). Similar lock-in mechanisms may exist for, noting as before, other receptors of the TNFR family (e.g., TNFR1, DR3, DR4, and DR5), as well as, observing their functional and structural homology, the PIDDosome, the octameric Dark-apoptosome in the fruit fly *Drosophila*, the tetrameric CED-4-apoptosome in the nematode *C. elegans*, and the inflammasome (Bao and Shi, 2007; Riedl and Salvesen, 2007; Tinel and Tschopp, 2004).

Concluding remarks

We have presented a mathematical model of death ligand-receptor interaction that strongly implicates Fas aggregation, e.g., through trimerization, in generating bistability at the level of the DISC. Naturally, this has profound consequences for apoptosis and therefore deserves further investigation. Our model assumptions of receptor clustering by FasL and of cluster-stabilization of open Fas should hence be verified, either, ideally, experimentally or by using atomistic simulations, e.g., molecular dynamics. Moreover, such properties should also be tested for functional homologues like other death receptors, as well as the PIDDosome, the apoptosome, and the inflammasome, as they may all share a conserved mode of operation. Furthermore, the current work has highlighted the critical role of receptor clustering, particularly in the context of pre-association, which enhances sensitivity to extrinsic apoptosis and additionally is upregulated by localization to lipid rafts (Muppidi et al., 2004). Therefore, future models of Fas signaling are likely to benefit from a spatial component modeling receptor distribution, which, in the continuum limit, generates a system of partial differential equations rather than the simpler ordinary differential equations presently considered. Finally, we hope that this study demonstrates the tremendous insight that can be provided by structural biology (see, e.g., Fesik, 2000), especially in collaboration with mathematical and computational modeling.

Materials and methods

Receptor density estimate

Approximating the cell as a cube of linear dimension $l \sim 10 \mu\text{m}$, the associated volume $v = l^3 \sim 1 \text{ pL}$ implies the correspondence $1 \text{ nM} \sim 600 \text{ molecules} \sim 10^{-6} \text{ molecules/nm}^2$ on restricting to the membrane, i.e., by averaging over the surface area $s = 6l^2 \sim 600 \mu\text{m}^2$. Thus, for a receptor concentration of 100 nM, the number of Fas molecules in the region about each receptor is only ~ 1 , assuming a square patch of size 100 nm.

Graphical notation

Models diagrams (Figures 1B, 4A, and 5A) follow the Systems Biology Graphical Notation (SBGN) and were drawn to comply with the SBGN Process Description language Level 1 (Le Novère et al., 2009).

Parameter selection

The baseline value of $n = 3$ was chosen for its biological relevance; the remaining parameters were set according to the following dimensional considerations. The characteristic Fas concentration is $s \sim 10$ nM, so the characteristic FasL concentration, estimated as its threshold concentration, is $l \sim 0.1$ nM (Bentele et al., 2004). Estimating $k_{-1} \sim 10^{-2} \text{ min}^{-1}$ gives a reaction rate of $v \sim 0.1$ nM/min for spontaneous receptor opening. Referencing the respective reactions against v hence gives $k_2 \sim 10^{-3} \text{ nM}^{-1} \text{ min}^{-1}$ and $k_l^{(2)} \sim 10^{-2} \text{ nM}^{-2} \text{ min}^{-1}$, so $\beta \sim 1$ and $\lambda \sim 10l \text{ nM}^{-1}$. Therefore, the nondimensional threshold ligand concentration is $\lambda_+ \sim 1$; we set α , γ , and δ , where intuitively $\alpha \gg 1$ and $\delta \ll 1$, to match this. Similarly, $k_4 \sim 0.1 \text{ nM}^{-1} \text{ min}^{-1}$, i.e., $\theta = 1$, but we set $\theta = 0$ for simplicity.

Steady-state solution

The steady states of the hysteron model are given by solving $d\zeta/d\tau = 0$, with each steady state classified as either stable if $d\zeta/d\tau|_{\zeta=\zeta_\infty} < 0$ and unstable otherwise (Box 1); this was done analytically if $\theta = 0$ and numerically otherwise.

Dynamic characterization

Trajectory families were generated under two conditions: first, by fixing FasL at $\lambda = 2.5$ (within the bistable regime) and imposing the initial conditions $(\xi^0, \eta^0, \zeta^0) = (1 - \zeta^0, 0, \zeta^0)$ for $0 \leq \zeta^0 \leq 1$; and second, by fixing $(\xi^0, \eta^0, \zeta^0) = (1, 0, 0)$ and letting $0 \leq \lambda \leq 10$. Integrations were performed at baseline parameter values (Table I) over $0 \leq \tau \leq 10^4$ using ODEPACK (Hindmarsh, 1983).

Asymptotic analysis

Solving $d\zeta/d\tau = 0$ for λ at $n = 3$ and $\theta = 0$ gives

$$\lambda = f_\lambda(\zeta_\infty) \equiv \frac{p_\lambda(\zeta_\infty)}{q_\lambda(\zeta_\infty)},$$

where p_λ and q_λ are polynomials of degrees two and three, respectively, so

$$\frac{\partial \lambda}{\partial \zeta_\infty} = f_{\partial \lambda / \partial \zeta}(\zeta_\infty) \equiv \frac{p_{\partial \lambda / \partial \zeta}(\zeta_\infty)}{q_{\partial \lambda / \partial \zeta}(\zeta_\infty)},$$

where $p_{\partial \lambda / \partial \zeta}$ and $q_{\partial \lambda / \partial \zeta}$ are of degrees four and six, respectively. The Fas activation and deactivation thresholds ζ_\pm are given by solving $\partial \lambda / \partial \zeta_\infty = 0$, i.e., $p_{\partial \lambda / \partial \zeta} = 0$. Assuming that $\zeta_\infty = \mathcal{O}(\varepsilon^\nu)$ with $\alpha = \mathcal{O}(1/\varepsilon)$, $\beta, \gamma = \mathcal{O}(1)$, and $\delta = \mathcal{O}(\varepsilon)$ for $\varepsilon \ll 1$, and balancing the orders of each pair of terms in $p_{\partial \lambda / \partial \zeta}$, we found the admissible values $\nu = 0$ and $1/2$ (Supplementary Table I). Solving the asymptotic forms of $p_{\partial \lambda / \partial \zeta}$ then gives $\zeta_+ = \mathcal{O}(\sqrt{\varepsilon})$ and $\zeta_- = \mathcal{O}(1)$ as the only nonnegative roots; the corresponding FasL thresholds are $\lambda_\pm = f_\lambda(\zeta_\pm)$.

Numerical computation of thresholds

Given α , β , γ , and δ , the bistability thresholds are computed by solving $p_{\partial \lambda / \partial \zeta}$ numerically for ζ_\pm and then computing $\lambda_\pm = f_\lambda(\zeta_\pm)$. If the ζ_\pm do not exist (i.e., all solutions are negative or complex), then we set $\zeta_\pm = 1/2$ and λ_\pm accordingly.

Log-normal distribution with scaled standard deviation

If $X \sim \text{Log-N}(\mu, \sigma^2)$, then the median and standard deviation of X are

$$\begin{aligned}\text{med}(X) &= e^\mu, \\ \text{std}(X) &= \sqrt{(e^{\sigma^2} - 1) e^{2\mu + \sigma^2}},\end{aligned}$$

respectively. Hence rescaling the standard deviation by defining $\chi = \text{std}(X)/\text{med}(X)$, i.e., the median analogue of the coefficient of variation,

$$\sigma = \sqrt{\log\left(\frac{1 + \sqrt{1 + 4\chi^2}}{2}\right)}.$$

Parameter generation for threshold analysis

For the threshold variation analysis, $N = 10^3$ parameter sets $(\alpha, \beta, \gamma, \delta)$ were drawn from a log-normal distribution with baseline median values (Table I) at $\chi = 0.25$ (Dataset 1). For the robustness of bistability analysis, we took χ at equally spaced points over $0 \leq \chi \leq 10$, at each similarly drawing N parameter sets about baseline values (Dataset 2).

Estimation of probability distributions

Probability distributions of parameters and thresholds were estimated using Gaussian kernel density estimation, with automatic bandwidth selection using the Scott factor (Scott, 1992).

Cell-level analysis

The cell-level analysis was performed using the data computed at $\chi = 0.25$ (Dataset 1), i.e., we partitioned the cell into $N = 10^3$ relay hysterons. The hysteresis curve was traced out by ranging FasL over $0 \leq \lambda \leq \lambda_+^{\max}$, where λ_+^{\max} is the maximum activation threshold over all parameters drawn, and then back, updating ζ_{cell} whenever a threshold is crossed.

Steady-state invariants

Gröbner bases were computed over $K = \mathbb{Z}(\mathbf{a})$ using the lexicographic monomial ordering (Box 3). For the hysteron invariant, we set $\lambda = \lambda_0$ and $\xi = 1 - \eta - \zeta$, hence expressing the dynamics $\mathbf{f} = \partial_\tau(\xi, \eta, \zeta)$ in terms of the variables $\mathbf{x} = (\eta, \lambda_0, \zeta)$; the variables are $\mathbf{a} = (\alpha, \beta, \gamma, \delta)$. We computed a Gröbner basis of $\langle \mathbf{f} \rangle$, from which elimination of η gives ω_H . Similarly, for the crosslinking invariant, we took $\lambda = \lambda_0 - \gamma_1 - \gamma_2 - \gamma_3$, $\rho = 1 - \zeta$, and $\gamma_1 = \zeta - 2\gamma_2 - 3\gamma_3$, and computed a Gröbner basis with $\mathbf{f} = \partial_\tau(\lambda, \rho, \gamma_1, \gamma_2, \gamma_3)$, $\mathbf{x} = (\gamma_2, \gamma_3, \lambda_0, \zeta)$, and $\mathbf{a} = \kappa$; eliminating γ_2 and γ_3 , we obtained ω_C .

Nonnegative least squares for model discrimination

Considering each term $\pm \lambda_0^i \zeta^j$ (with sign chosen as appropriate) in ω_H and ω_C as an independent variable, we split the associated constant c_{ij} into variable and constant parts $c_{ij}^{\text{var}}(\mathbf{a})$ and c_{ij}^{const} , respectively, so that $c_{ij}^{\text{var}} \geq 0$, assuming the asymptotic ordering $\alpha = \mathcal{O}(1/\epsilon)$, $\beta, \gamma = \mathcal{O}(1)$, and $\delta = \mathcal{O}(\epsilon)$ for $\epsilon \ll 1$, with $\Delta > 1$. The required optimization is then a nonnegative least squares problem (Lawson and Hanson, 1995) minimizing $\epsilon = \|Uc^{\text{var}} + Uc^{\text{const}}\|_2$, suppressing model reference for generality, where $U = (u_1, \dots, u_N)$ is a matrix of experimental data, for each u_i a row vector corresponding to an experimental trial; $c^{\text{var}} = (c_{ij}^{\text{var}})$

is a column vector of nonnegative coefficients to be determined; and $c^{\text{const}} = (c_{ij}^{\text{const}})$ is a column vector of constants.

Parameter generation for model discrimination

Parameters were randomly drawn for each model using the following procedure. The initial FasL concentration λ^0 was sampled from a log-normal distribution with median $\text{med}(\lambda_{\text{H}}^0) = 2.5$ and $\text{med}(\lambda_{\text{C}}^0) = 0.25$ for the hysteron and crosslinking models, respectively (FasL is nondimensionalized differently in the two models), and scaled standard deviation $\chi(\lambda^0) = 1$. The concentrations of the remaining species, which are all constrained by nondimensionalization, were then drawn uniformly in sequence over the appropriate range, i.e., for the hysteron model, we sampled $\xi^0 \in [0, 1]$, then $\eta^0 \in [0, 1 - \xi^0]$, then $\zeta^0 \in [0, 1 - \xi^0 - \eta^0]$, while for the crosslinking model, we took $\rho^0 \in [0, 1]$, next $\gamma_1^0 \in [0, 1 - \rho^0]$, then $\gamma_2^0 \in [0, (1 - \rho^0 - \gamma_1^0)/2]$, and finally $\gamma_3^0 \in [0, (1 - \rho^0 - \gamma_1^0 - 2\gamma_2^0)/3]$. Steady-state experimental data were obtained for each parameter set by solving the steady-state equations governing each model and making the identifications $\lambda_0 = \lambda_\infty$ for the hysteron model, and $\lambda_0 = \lambda_\infty + \gamma_{1,\infty} + \gamma_{2,\infty} + \gamma_{3,\infty}$ and $\zeta_\infty = \gamma_{1,\infty} + 2\gamma_{2,\infty} + 3\gamma_{3,\infty}$ for the crosslinking model. For each model, $N = 100$ parameter sets were drawn (Datasets 3 and 4).

SBML implementation

For standards compliance, the hysteron and hysteron-caspase models were implemented in dimensional form using the Systems Biology Markup Language (SBML) Level 2 Version 1 (Finney and Hucka, 2003; Hucka et al., 2003). The models and sample analyses performed on them are given in the Supplementary Information (Supplementary Note 5).

Computational software

All calculations in the main paper were performed using Sage 4.2.1 (<http://www.sagemath.org/>), supplemented with NumPy/SciPy (<http://www.scipy.org/>; Oliphant, 2007) for numerical computation and matplotlib (Hunter, 2007) for data visualization. The Sage worksheet containing all computations described is provided in the Supplementary Information and can also be downloaded from <http://www.sagenb.org/home/pub/1224/> or <http://www.courant.nyu.edu/~ho/>. Some supporting calculations in the Supplementary Information were performed in MATLAB (The MathWorks, Inc., Natick, MA, USA) using SBTOOL-BOX2 (Schmidt and Jirstrand, 2006) and SBML-SAT (Zi et al., 2008).

Acknowledgements

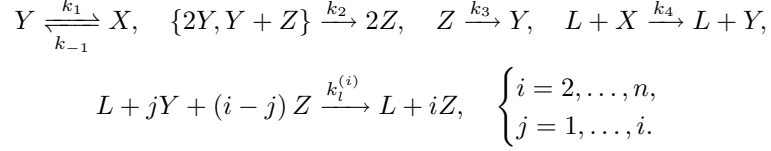
We thank Leslie Greengard and the Courant Institute for hosting and facilitating our research. KLH acknowledges support from the NYU MacCracken and NSF IGERT (DGE 0333389) programs. HAH acknowledges support from an IC Deputy Rector’s Award, the IC Department of Mathematics, and a NSF Graduate Research Fellowship.

Boxes

Box 1. Hysteron model equations and solution

Posit three species of Fas according to their conformational states: closed (X); open, unstable (Y); and open, stable (Z), i.e., active and signaling. Furthermore, let the ligand FasL be denoted by L . For a general

clustering parameter n , giving the maximum number of receptors that each ligand can coordinate, assign the reactions



The first reaction describes spontaneous receptor opening and closing. The second reaction describes pairwise stabilization by open Fas, irrespective of the presence of FasL; higher-order analogues, though in principle available, are neglected as justified by the low estimated receptor density. The third reaction describes the constitutive destabilization of open Fas; and the fourth, ligand-induced receptor opening. Finally, the fifth reaction captures all cluster-stabilization events enabled by FasL, the order being limited by n .

Under the convention that lowercase letters denote the concentrations of their uppercase counterparts, the model dynamics, as given by mass action, are

$$\frac{dx}{dt} = v_1 - v_4, \quad \frac{dy}{dt} = -v_1 - v_2 + v_3 + v_4 - v_l, \quad \frac{dz}{dt} = v_2 - v_3 + v_l,$$

where

$$v_1 = k_1 y - k_{-1} x, \quad v_2 = 2k_2 y^2 + k_2 y z, \quad v_3 = k_3 z, \quad v_4 = k_4 l x, \quad v_l = l \sum_{i=2}^n k_l^{(i)} \sum_{j=1}^i j y^j z^{i-j}.$$

Clearly, ligand is conserved and so may be treated as a parameter. We rescale the system by introducing the nondimensional variables

$$\xi = \frac{x}{s}, \quad \eta = \frac{y}{s}, \quad \zeta = \frac{z}{s}, \quad \lambda = \frac{k_l^{(2)} l s}{k_{-1}}, \quad \tau = k_{-1} t,$$

where $s \equiv x + y + z$ is the conserved receptor concentration. Further, let

$$\alpha = \frac{k_1}{k_{-1}}, \quad \beta = \frac{k_2 s}{k_{-1}}, \quad \delta = \frac{k_3}{k_{-1}}, \quad \theta = \frac{k_4}{k_l^{(2)} s},$$

and, for simplicity, enforce the uniformity condition

$$\gamma = \frac{k_l^{(i)} s^{i-2}}{k_l^{(2)}}, \quad i = 3, \dots, n.$$

Then at steady state, denoted by the subscript ∞ ,

$$\xi_\infty = \frac{\alpha \eta_\infty}{1 + \theta \lambda}, \quad \eta_\infty = \frac{1 - \zeta_\infty}{1 + \alpha / (1 + \theta \lambda)},$$

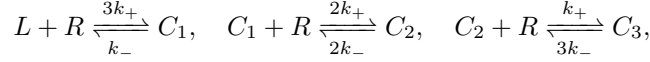
so ζ_∞ is given by considering

$$\frac{d\zeta}{d\tau} = 2(\beta + \lambda)\eta^2 + (\beta + \lambda)\eta\zeta + \gamma\lambda \sum_{i=3}^n \sum_{j=1}^i j \eta^j \zeta^{i-j} - \delta\zeta$$

and solving $d\zeta/d\tau = 0$ with $\eta \mapsto \eta_\infty$ and $\zeta \mapsto \zeta_\infty$, a polynomial equation in ζ_∞ of degree n .

Box 2. Crosslinking model equations and solution

We assume five species: FasL (L), Fas (R), and the complexes FasL:Fas (C_1), FasL:Fas₂ (C_2), and FasL:Fas₃ (C_3). These obey the reactions



which describe the independent recruitment of Fas at each of three binding sites by FasL; note that the reaction rates have been adjusted for combinatorial factors. The dynamics are

$$\frac{dl}{dt} = -v_1, \quad \frac{dr}{dt} = -v_1 - v_2 - v_3, \quad \frac{dc_1}{dt} = v_1 - v_2, \quad \frac{dc_2}{dt} = v_2 - v_3, \quad \frac{dc_3}{dt} = v_3,$$

where

$$v_1 = 3k_+lr - k_-c_1, \quad v_2 = 2k_+c_1r - 2k_-c_2, \quad v_3 = k_+c_2r - 3k_-c_3.$$

Nondimensionalize by setting

$$\lambda = \frac{l}{r_0}, \quad \rho = \frac{r}{r_0}, \quad \gamma_i = \frac{c_i}{r_0}, \quad \tau = k_-t, \quad \kappa = \frac{k_-}{k_+r_0},$$

where r_0 is the total receptor concentration. In these variables, the system admits the conservation relations

$$\lambda_0 = \lambda + \gamma_1 + \gamma_2 + \gamma_3, \quad 1 = \rho + \gamma_1 + 2\gamma_2 + 3\gamma_3,$$

interpreted as ligand and receptor conservation, respectively. At steady state,

$$\gamma_{1,\infty} = 3\lambda_\infty \left(\frac{\rho_\infty}{\kappa} \right), \quad \gamma_{2,\infty} = 3\lambda_\infty \left(\frac{\rho_\infty}{\kappa} \right)^2, \quad \gamma_{3,\infty} = \lambda_\infty \left(\frac{\rho_\infty}{\kappa} \right)^3,$$

where

$$\lambda_\infty = \frac{\lambda_0}{1 + 3(\rho_\infty/\kappa) + 3(\rho_\infty/\kappa)^2 + (\rho_\infty/\kappa)^3}$$

and

$$\rho_\infty = \frac{1}{2} \left[\sqrt{(3\lambda_0 + \kappa - 1)^2 + 4\kappa} - (3\lambda_0 + \kappa - 1) \right].$$

Box 3. Steady-state invariants using Gröbner bases

We give a brief overview of the relevant mathematics below; for details, see, e.g., Cox et al. (2007). For convenience, we will use boldface notation to denote both vectors and sets interchangeably as appropriate, the precise meaning to be understood from the context.

Let $\mathbf{f} = (f_1, \dots, f_m) \in K[\mathbf{x}]$ be a system of polynomials in $\mathbf{x} = (x_1, \dots, x_n)$ with coefficients from a field K . For our purposes, \mathbf{f} is a set of mass-action dynamics, where \mathbf{x} is a set of species concentrations, and K is, e.g., the real numbers \mathbb{R} ; or the field $\mathbb{R}(\mathbf{a})$ of rational functions in the kinetic parameters $\mathbf{a} = (a_1, \dots, a_k)$ with coefficients in \mathbb{R} ; or the field $\mathbb{Z}(\mathbf{a})$ of rational functions in \mathbf{a} with coefficients in the integers \mathbb{Z} . Consider the variety $V = \{\mathbf{x} \in K^n : \mathbf{f}(\mathbf{x}) = \mathbf{0}\}$ on which \mathbf{f} vanishes—this is simply the set of steady states of \mathbf{f} —and let $I = \langle \mathbf{f} \rangle$ be the ideal generated by \mathbf{f} , containing all polynomials of the form $\sum_{i=1}^m f_i h_i$, where the $h_i \in K[\mathbf{x}]$ are arbitrary polynomials. Clearly, I consists of all polynomials in $K[\mathbf{x}]$ that vanish on V . Thus,

I is invariant on and hence characterizes V , in particular, through the requirement that for any $\mathbf{x} \in V$, $h(\mathbf{x}) = 0$ for all $h \in I$.

The elements f_1, \dots, f_m of \mathbf{f} form a basis for I . This basis is not unique; notably, we may express $I = \langle \mathbf{g} \rangle$ in terms of a Gröbner basis $\mathbf{g} = (g_1, \dots, g_l)$, which has particularly useful properties, chief among them, for this application, the *elimination property*, which states that, relative to the lexicographic ordering $x_1 > \dots > x_n$, the elimination ideal $\tilde{I} = I \cap K[\tilde{\mathbf{x}}]$ of I containing only the variables $\tilde{\mathbf{x}} = (x_{i+1}, \dots, x_n)$ is simply $\tilde{I} = \langle \mathbf{g} \cap K[\tilde{\mathbf{x}}] \rangle$. Gröbner bases thus give a straightforward method of computing elimination ideals, which may be useful, for example, if the concentrations of certain molecular species x_1, \dots, x_i cannot be measured experimentally and hence, in principle, must remain unknown. The generators $\tilde{\mathbf{g}} = \mathbf{g} \cap K[\tilde{\mathbf{x}}]$ of \tilde{I} then constitute experimentally measurable steady-state invariants of the system, i.e., $\tilde{\mathbf{g}}(\tilde{\mathbf{x}}) = \mathbf{0}$ for all $\tilde{\mathbf{x}} \in \tilde{V}$, where \tilde{V} is the projection of V onto the coordinates $\tilde{\mathbf{x}}$.

In the current context, since \mathbf{f} comes from mass action, we will work over $K = \mathbb{Z}(\mathbf{a})$, thus treating parameters symbolically and hence allowing the derivation of invariants valid for all choices of \mathbf{a} .

Gröbner bases are a standard tool in computational algebraic geometry and can be computed by many software packages, including Maple (Waterloo Maple Inc., Waterloo, Ontario, Canada), Mathematica (Wolfram Research, Inc., Champaign, IL, USA), and Sage (<http://www.sagemath.org/>).

Box 4. Feedforward caspase model equations and solution

Posit the inactive caspase zymogens procaspase-8 (Casp8) and procaspase-3 (Casp3), and their corresponding active forms caspase-8 (Casp8*) and caspase-3 (Casp3*). Caspase-3 represents all effector caspases in the system, so its concentration will be considered a measure of the degree of apoptotic activation. The model reactions are



where the first reaction describes the activation of caspase-8; and the second, the activation of caspase-3. In general, Z denotes a death signal such as the DISC, but in our application will refer to active Fas, so as to provide a link to the hysteron and crosslinking models. For reasons of stability, we further supplement with the constitutive synthesis and degradation reactions



which we take as symmetric for simplicity.

Letting

$$x = [\text{Casp8}], \quad x^* = [\text{Casp8}^*], \quad y = [\text{Casp3}], \quad y^* = [\text{Casp3}^*],$$

the dynamics are

$$\frac{dx}{dt} = -v_1 + v_x, \quad \frac{dx^*}{dt} = v_1 - v_{x^*}, \quad \frac{dy}{dt} = -v_2 + v_y, \quad \frac{dy^*}{dt} = v_2 - v_{y^*},$$

where

$$v_1 = k_1 x z, \quad v_2 = k_2 x^* y, \quad \left\{ \begin{array}{c} v_x \\ v_y \end{array} \right\} = k_3 - k_{-3} \left\{ \begin{array}{c} x \\ y \end{array} \right\}, \quad \left\{ \begin{array}{c} v_{x^*} \\ v_{y^*} \end{array} \right\} = k_4 \left\{ \begin{array}{c} x^* \\ y^* \end{array} \right\}.$$

Define $\Omega = k_3/k_{-3}$ and $\sigma = s/\Omega$, i.e., the equilibrium procaspase and relative receptor concentrations, respectively, and let

$$\phi = \frac{x}{\Omega}, \quad \phi^* = \frac{x^*}{\Omega}, \quad \psi = \frac{y}{\Omega}, \quad \psi^* = \frac{y^*}{\Omega}.$$

Then expressing the dynamics in terms of

$$\pi_\phi = \frac{k_1\Omega}{k_{-3}}, \quad \pi_\psi = \frac{k_2\Omega}{k_{-3}}, \quad \pi_\delta = \frac{k_4}{k_{-3}}, \quad \tau = k_{-3}t,$$

we obtain, at steady state,

$$\phi_\infty = \frac{1}{1 + \pi_\phi\sigma\zeta}, \quad \phi_\infty^* = \frac{1 - \phi_\infty}{\pi_\delta}, \quad \psi_\infty = \frac{1}{1 + \pi_\psi\phi_\infty^*}, \quad \psi_\infty^* = \frac{1 - \psi_\infty}{\pi_\delta}.$$

References

- Abeck JG, Burke JM, Aldridge BB, Zhang M, Lauffenburger DA, Sorger PK (2008a) Quantitative analysis of pathways controlling extrinsic apoptosis in single cells. *Mol Cell* **30**: 11–25
- Abeck JG, Burke JM, Spencer SL, Lauffenburger DA, Sorger PK (2008b) Modeling a snap-action, variable-delay switch controlling extrinsic cell death. *PLoS Biol* **6**: e299
- Apgar JF, Toettcher JE, Endy D, White FM, Tidor B (2008) Stimulus design for model selection and validation in cell signaling. *PLoS Comput Biol* **4**: e30
- Ashkenazi A, Dixit VM (1998) Death receptors: Signaling and modulation. *Science* **281**: 1305–1308
- Bagci EZ, Vodovotz Y, Billiar TR, Ermentrout GB, Bahar I (2006) Bistability in apoptosis: Roles of Bax, Bcl-2, and mitochondrial permeability transition pores. *Biophys J* **90**: 1546–1559
- Bao Q, Shi Y (2007) Apoptosome: a platform for the activation of initiator caspases. *Cell Death Differ* **14**: 56–65
- Barker JA, Schreiber DE, Huth BG, Everett DH (1983) Magnetic hysteresis and minor loops: Models and experiments. *Proc R Soc Lond A* **386**: 251–261
- Bentele M, Lavrik I, Ulrich M, Stößer S, Heermann D, Kalthoff H, Krammer P, Eils R (2004) Mathematical modeling reveals threshold mechanism in CD95-induced apoptosis. *J Cell Biol* **166**: 839–851
- Budihardjo I, Oliver H, Lutter M, Luo X, Wang X (1999) Biochemical pathways of caspase activation during apoptosis. *Annu Rev Cell Dev Biol* **15**: 269–290
- Cain K, Bratton SB, Cohen GM (2002) The Apaf-1 apoptosome: a large caspase-activating complex. *Biochimie* **84**: 203–214
- Chan FKM (2007) Three is better than one: Pre-ligand receptor assembly in the regulation of TNF receptor signaling. *Cytokine* **37**: 101–107
- Chan FKM, Chun HJ, Zheng L, Siegel RM, Bui KL, Lenardo MJ (2000) A domain in TNF receptors that mediates ligand-independent receptor assembly and signaling. *Science* **288**: 2351–2354
- Chan FKM, Siegel RM, Zacharias DA, Swofford R, Holmes KL, Tsien RY, Lenardo MJ (2001) Fluorescence resonance energy transfer analysis of cell surface receptor interactions and signaling using spectral variants of the green fluorescent protein. *Cytometry* **44**: 361–368
- Cowling V, Downward J (2002) Caspase-6 is the direct activator of caspase-8 in the cytochrome *c*-induced apoptosis pathway: absolute requirement for removal of caspase-6 prodomain. *Cell Death Differ* **9**: 1046–1056

- Cox D, Little J, O’Shea D (2007) *Ideals, Varieties, and Algorithms: An Introduction to Computational Algebraic Geometry and Commutative Algebra*. 3rd ed. Springer-Verlag, New York, NY, USA
- Cui J, Chen C, Lu H, Sun T, Shen P (2008) Two independent positive feedbacks and bistability in the Bcl-2 apoptotic switch. *PLoS ONE* **3**: e1469
- Danial NN, Korsmeyer SJ (2004) Cell death: Critical control points. *Cell* **116**: 205–219
- Eißing T, Allgöwer F, Bullinger E (2005) Robustness properties of apoptosis models with respect to parameter variations and intrinsic noise. *IEE Proc Syst Biol* **152**: 221–228
- Eißing T, Conzelmann H, Gilles ED, Allgöwer F, Bullinger E, Scheurich P (2004) Bistability analyses of a caspase activation model for receptor-induced apoptosis. *J Biol Chem* **279**: 36892–36897
- Faugère JC (1999) A new efficient algorithm for computing Gröbner bases (F4). *J Pure Appl Algebra* **139**: 61–88
- Faugère JC (2002) A new efficient algorithm for computing Gröbner bases without reduction to zero (F5). In *Proceedings of the 2002 International Symposium on Symbolic and Algebraic Computation*, International Conference on Symbolic and Algebraic Computation, pp. 75–83. Association for Computing Machinery, New York, NY, USA
- Faugère JC, Hering M, Phan J (2003) The membrane inclusions curvature equations. *Adv Appl Math* **31**: 643–658
- Fesik SW (2000) Insights into programmed cell death through structural biology. *Cell* **103**: 273–282
- Finney A, Hucka M (2003) Systems biology markup language: Level 2 and beyond. *Biochem Soc Trans* **31**: 1472–1473
- Fulda S, Debatin KM (2006) Extrinsic versus intrinsic apoptosis pathways in anticancer chemotherapy. *Oncogene* **25**: 4798–4811
- Fumarola C, Guidotti GG (2004) Stress-induced apoptosis: Toward a symmetry with receptor-mediated cell death. *Apoptosis* **9**: 77–82
- Fussenegger M, Bailey JE, Varner J (2000) A mathematical model of caspase function in apoptosis. *Nat Biotechnol* **18**: 768–774
- Harrington HA, Ho KL, Ghosh S, Tung K (2008) Construction and analysis of a modular model of caspase activation in apoptosis. *Theor Biol Med Model* **5**: 26
- Hindmarsh AC (1983) ODEPACK: a systematized collection of ODE solvers. In Stepleman RS, Carver M, Peskin R, Ames WF, Vichnevetsky R (eds.) *Scientific Computing*, vol. 1 of *IMACS Transactions on Scientific Computation*, pp. 55–64. North-Holland, Amsterdam, The Netherlands
- Hua F, Cornejo MG, Cardone MH, Stokes CL, Lauffenburger DA (2005) Effects of Bcl-2 levels on Fas signaling-induced caspase-3 activation: Molecular genetic tests of computational model predictions. *J Immunol* **175**: 985–995
- Hua F, Hautaniemi S, Yokoo R, Lauffenburger DA (2006) Integrated mechanistic and data-driven modelling for multivariate analysis of signalling pathways. *J R Soc Interface* **3**: 515–526

- Hucka M, Finney A, Sauro HM, Bolouri H, Doyle JC, Kitano H, Arkin AP, Bornstein BJ, Bray D, Cornish-Bowden A, Cueller AA, Dronov S, Gilles ED, Ginkel M, Gor V, Goryanin II, Hedley WJ, Hodgman TC, Hofmeyr JH, Hunter PJ, et al. (2003) The systems biology markup language (SBML): a medium for representation and exchange of biochemical network models. *Bioinformatics* **19**: 524–531
- Hunter JD (2007) Matplotlib: A 2D graphics environment. *Comput Sci Eng* **9**: 90–95
- Ising E (1925) Beitrag zur theorie des ferromagnetismus. *Z Phys* **31**: 253–258
- Janes KA, Albeck JG, Gaudet S, Sorger PK, Lauffenburger DA, Yaffe MB (2005) A systems model of signaling identifies a molecular basis set for cytokine-induced apoptosis. *Science* **310**: 1646–1653
- Kerr JFR, Wyllie AH, Currie AR (1972) Apoptosis: a basic biological phenomenon with wide-ranging implications in tissue kinetics. *Br J Cancer* **26**: 239–257
- Kitano H (2004) Biological robustness. *Nat Rev Genet* **5**: 826–837
- Lai R, Jackson TL (2004) A mathematical model of receptor-mediated apoptosis: dying to know why FasL is a trimer. *Math Biosci Eng* **1**: 325–328
- Lawson CL, Hanson RJ (1995) *Solving Least Squares Problems*. Society for Industrial and Applied Mathematics, Philadelphia, PA, USA
- Le Novère N, Hucka M, Mi H, Moodie S, Schreiber F, Sorokin A, Demir E, Wegner K, Aladjem MI, Wimalaratne SM, Bergman FT, Gauges R, Ghazal P, Kawaji H, Li L, Matsuoka Y, Villéger A, Boyd SE, Calzone L, Courtot M, et al. (2009) The systems biology graphical notation. *Nat Biotechnol* **27**: 735–741
- Legewie S, Blüthgen N, Herzog H (2006) Mathematical modeling identifies inhibitors of apoptosis as mediators of positive feedback and bistability. *PLoS Comput Biol* **2**: e120
- Manrai AK, Gunawardena J (2008) The geometry of multisite phosphorylation. *Biophys J* **95**: 5533–5543
- Meier P, Finch A, Evan G (2000) Apoptosis in development. *Nature* **407**: 796–801
- Muppidi JR, Siegel RM (2004) Ligand-independent redistribution of Fas (CD95) into lipid rafts mediates clonotypic T cell death. *Nat Immunol* **5**: 182–189
- Muppidi JR, Tschopp J, Siegel RM (2004) Life and death decisions: Secondary complexes and lipid rafts in TNF receptor family signal transduction. *Immunity* **21**: 461–465
- Nakabayashi J, Sasaki A (2006) A mathematical model for apoptosome assembly: The optimal cytochrome *c*/Apaf-1 ratio. *J Theor Biol* **242**: 280–287
- Neun W, Melenk H (1992) Very large Gröbner basis calculations. In *Proceedings of the Second International Workshop on Computer Algebra and Parallelism*, vol. 584 of *Lecture Notes in Computer Science*, pp. 89–99. Springer-Verlag, London, UK
- Nicholson DW (1999) Caspase structure, proteolytic substrates, and function during apoptotic cell death. *Cell Death Differ* **6**: 1028–1042
- Nicholson DW, Thornberry NA (1997) Caspases: killer proteases. *Trends Biochem Sci* **22**: 299–306
- Núñez G, Benedict MA, Hu Y, Inohara N (1998) Caspases: the proteases of the apoptotic pathway. *Oncogene* **17**: 3237–3245

- Okazaki N, Asano R, Kinoshita T, Chuman H (2008) Simple computational models of type I/type II cells in Fas signaling-induced apoptosis. *J Theor Biol* **250**: 621–633
- Oliphant TE (2007) Python for scientific computing. *Comput Sci Eng* **9**: 10–20
- Peter ME, Krammer PH (1998) Mechanisms of CD95 (APO-1/Fas)-mediated apoptosis. *Curr Opin Immunol* **10**: 545–551
- Peter ME, Krammer PH (2003) The CD95(APO-1/Fas) DISC and beyond. *Cell Death Differ* **10**: 26–35
- Preisach F (1935) Über die magnetische nachwirkung. *Z Phys* **94**: 277–302
- Raff M (1998) Cell suicide for beginners. *Nature* **396**: 119–122
- Rangamani P, Sirovich L (2007) Survival and apoptotic pathways initiated by TNF- α : Modeling and predictions. *Biotechnol Bioeng* **97**: 1216–1229
- Riedl SJ, Salvesen GS (2007) The apoptosome: signalling platform of cell death. *Nat Rev Mol Cell Biol* **8**: 405–413
- Ryu S, Lin S, Ugel N, Antoniotti M, Mishra B (2008) Mathematical modeling of the formation of apoptosome in intrinsic pathway of apoptosis. *Syst Synth Biol* **2**: 49–66
- Schmidt H, Jirstrand M (2006) Systems Biology Toolbox for MATLAB: a computational platform for research in systems biology. *Bioinformatics* **22**
- Scott DW (1992) *Multivariate Density Estimation: Theory, Practice, and Visualization*. John Wiley & Sons, Inc., New York, NY, USA
- Scott FL, Stec B, Pop C, Dobaczewska MK, Lee JJ, Monosov E, Robinson H, Salvesen GS, Schwarzenbacher R, Riedl SJ (2009) The Fas-FADD death domain complex structure unravels signalling by receptor clustering. *Nature* **457**: 1019–1022
- Siegel RM, Frederiksen JK, Zacharias DA, Chan FKM, Johnson M, Lynch D, Tsien RY, Lenardo MJ (2000) Fas preassociation required for apoptosis signaling and dominant inhibition by pathogenic mutations. *Science* **288**: 2354–2357
- Slee EA, Harte MT, Kluck RM, Wolf BB, Casiano CA, Newmeyer DD, Wang HG, Reed JC, Nicholson DW, Alnemri ES, Green DR, Martin SJ (1999) Ordering the cytochrome *c*-initiated caspase cascade: Hierarchical activation of caspases-2, -3, -6, -7, -8, and -10 in a caspase-9-dependent manner. *J Cell Biol* **144**: 281–292
- Stucki JW, Simon HU (2005) Mathematical modeling of the regulation of caspase-3 activation and degradation. *J Theor Biol* **234**: 123–131
- Taylor RC, Cullen SP, Martin SJ (2008) Apoptosis: controlled demolition at the cellular level. *Nat Rev Mol Cell Biol* **9**: 231–241
- Thompson CB (1995) Apoptosis in the pathogenesis and treatment of disease. *Science* **267**: 1456–1462
- Thornberry NA, Lazebnik Y (1998) Caspases: Enemies within. *Science* **281**: 1312–1316
- Tinel A, Tschopp J (2004) The PIDDosome, a protein complex implicated in activation of caspase-2 in response to genotoxic stress. *Science* **304**: 843–846

- Wyllie AH, Kerr JFR, Currie AR (1980) Cell death: the significance of apoptosis. *Int Rev Cytol* **68**: 251–306
- Yu X, Acehan D, Ménétret JF, Booth CR, Ludtke SJ, Riedl SJ, Shi Y, Wang X, Akey CW (2005) A structure of the human apoptosome at 12.8 Å resolution provides insights into this cell death platform. *Structure* **13**: 1725–1735
- Zi Z, Zheng Y, Rundell AE, Klipp E (2008) SBML-SAT: a systems biology markup language (SBML) based sensitivity analysis tool. *BMC Bioinformatics* **9**: 342

The Fas trimer hysteron model: bistability in apoptosis from receptor clustering (Supplementary Information)

Kenneth L. Ho^{1,2} and Heather A. Harrington^{3,4}

¹Courant Institute of Mathematical Sciences, New York University, New York, NY, USA

²Program in Computational Biology, New York University, New York, NY, USA

³Department of Mathematics, Imperial College London, London, UK

⁴Centre for Integrative Systems Biology at Imperial College, Imperial College London, London, UK

Contents

1	Bistability thresholds and robustness	1
1.1	Asymptotic analysis	1
1.2	Threshold variation data statistics	4
1.3	Discrete variation analysis for robustness of bistability	4
2	Parameter identification	6
3	Stochastic simulation	7
4	Comparison with the crosslinking model	7
4.1	Solution of crosslinking model	7
4.2	Steady-state invariants	9
4.3	Nonnegative least squares for model discrimination	9
4.4	Performance of model discrimination	10
5	SBML implementation	11
5.1	Model definition	11
5.2	Sensitivity analysis	11
5.3	Robustness analysis	13
6	Datasets	13

1 Bistability thresholds and robustness

1.1 Asymptotic analysis

The activation and deactivation thresholds λ_{\pm} that define the bistable regime are given by the values of λ at which $\partial\lambda/\partial\zeta_{\infty} = 0$. As mentioned in the main paper, we restricted to the biological context of $n = 3$ and

Supplementary Table I Order balance of $p_{\partial\lambda/\partial\zeta} = \sum_{i=0}^4 c_i \zeta_\infty^i$. Top, critical values of ν , where $\zeta_\infty = \mathcal{O}(\varepsilon^\nu)$ for $\varepsilon \ll 1$, balancing each pair of terms in $p_{\partial\lambda/\partial\zeta}$; bottom, corresponding ε -exponent of the order of each term. Admissible balances are enclosed in parenthesis.

	$c_4 = \mathcal{O}(\varepsilon^{4\nu-4})$	$c_3 = \mathcal{O}(\varepsilon^{3\nu-4})$	$c_2 = \mathcal{O}(\varepsilon^{2\nu-4})$	$c_1 = \mathcal{O}(\varepsilon^{\nu-3})$	$c_0 = \mathcal{O}(\varepsilon^{-3})$
c_4	—	0	0	1/3	1/4
c_3		—	0	1/2	1/3
c_2			—	1	1/2
c_1				—	0
c_0					—
1	0	-1	-2	-2	-3
(1/2)	-2	-5/2	(-3)	-5/2	(-3)
1/3	-8/3	-3	-10/3	-8/3	-3
1/4	-3	-13/4	-7/2	-11/4	-3
(0)	(-4)	(-4)	(-4)	-3	-3

further fixed $\theta = 0$. Thus, solving $d\zeta/d\tau = 0$ gives

$$\lambda = f_\lambda(\zeta_\infty) \equiv \frac{p_\lambda(\zeta_\infty)}{q_\lambda(\zeta_\infty)},$$

where p_λ and q_λ are polynomials of degrees two and three, respectively, hence

$$\frac{\partial\lambda}{\partial\zeta_\infty} = f_{\partial\lambda/\partial\zeta}(\zeta_\infty) \equiv \frac{p_{\partial\lambda/\partial\zeta}(\zeta_\infty)}{q_{\partial\lambda/\partial\zeta}(\zeta_\infty)},$$

where $p_{\partial\lambda/\partial\zeta}$ and $q_{\partial\lambda/\partial\zeta}$ are polynomials of degrees four and six, respectively. Since we are concerned with $\partial\lambda/\partial\zeta_\infty = 0$, we considered only $p_{\partial\lambda/\partial\zeta}$ in solving for λ_\pm . The strategy then is to solve $p_{\partial\lambda/\partial\zeta}$ for the Fas thresholds ζ_\pm , then to compute $\lambda_\pm = f_\lambda(\zeta_\pm)$.

In the asymptotic limit

$$\alpha = \mathcal{O}\left(\frac{1}{\varepsilon}\right), \quad \beta, \gamma = \mathcal{O}(1), \quad \delta = \mathcal{O}(\varepsilon) \quad (1)$$

for $\varepsilon \ll 1$,

$$p_\lambda(\zeta) \sim -\alpha^2\beta\zeta^2 - \alpha^2(\alpha\delta - \beta)\zeta + 2\alpha\beta, \quad q_\lambda(\zeta) \sim \alpha^2\gamma\zeta^3 - \alpha^2(\gamma - 1)\zeta^2 - \alpha^2\zeta - 2\alpha,$$

and

$$p_{\partial\lambda/\partial\zeta}(\zeta) \sim \alpha^4\beta\gamma\zeta^4 + 2\alpha^4(\alpha\delta - \beta)\gamma\zeta^3 - \alpha^2[(\alpha\delta - \beta)\gamma - \alpha\delta]\zeta^2 + 4\alpha^3\beta\gamma\zeta + 2\alpha^4\delta$$

on asymptotically expanding each coefficient. Thus, suppose that $\zeta_\infty = \mathcal{O}(\varepsilon^\nu)$ and find the critical values of ν that balance the orders of each pair of terms in $p_{\partial\lambda/\partial\zeta}$. Clearly, the values of ν such that only one dominant term exists must be discounted, hence we obtained the admissible values $\nu = 0$ and $1/2$ (Supplementary Table I).

For $\nu = 1/2$,

$$p_{\partial\lambda/\partial\zeta}(\zeta) \sim -\alpha^4\gamma(\alpha\delta - \beta)\delta\zeta^2 + 2\alpha^4\delta,$$

so

$$\zeta_+ \sim \sqrt{\frac{2\Delta}{\alpha[\gamma(\Delta-1)-\Delta]}} \quad (2)$$

is the unique nonnegative root, provided that $\gamma > 1$ and $\Delta > \gamma/(\gamma-1)$, where, recall,

$$\Delta = \frac{\alpha\delta}{\beta} = \mathcal{O}(1) \quad (3)$$

is the relative intrinsic deactivation strength. Similarly, for $\nu = 0$,

$$p_{\partial\lambda/\partial\zeta}(\zeta) \sim \alpha^4\beta\gamma\zeta^4 + 2\alpha^4(\alpha\delta - \beta)\gamma\zeta^3 - \alpha^4[(\alpha\delta - \beta)\gamma - \alpha\delta]\zeta^2,$$

so

$$\zeta_- \sim \sqrt{\frac{\Delta\Theta}{\gamma}} - (\Delta - 1), \quad (4)$$

where

$$\Theta = \gamma(\Delta - 1) - 1 = \mathcal{O}(1), \quad (5)$$

which exists if $\Theta \geq 0$, i.e., $\Delta \geq 1 + 1/\gamma$; note that the trivial root $\zeta_\infty \sim 0$ of multiplicity two recovers the solutions of order $\mathcal{O}(\sqrt{\varepsilon})$. As physical intuition demands, $p_{\partial\lambda/\partial\zeta}$ has at most two nonnegative roots, which both exist if

$$\Delta > \Delta^* \equiv \max\left\{\frac{\gamma}{\gamma-1}, \frac{\gamma+1}{\gamma}\right\} > 1, \quad (6)$$

given $\gamma > 1$.

Clearly, the ζ_\pm give, under the map f_λ , the activation and deactivation thresholds λ_\pm , respectively. Proceeding first with $\zeta_+ = \mathcal{O}(\sqrt{\varepsilon})$,

$$p_\lambda(\zeta_+) \sim -\alpha^2(\alpha\delta - \beta)\zeta_+, \quad q_\lambda(\zeta_+) \sim -\alpha^2\zeta_+,$$

so

$$\lambda_+ = f_\lambda(\zeta_+) \sim \beta(\Delta - 1). \quad (7)$$

Similarly, for $\zeta_- = \mathcal{O}(1)$,

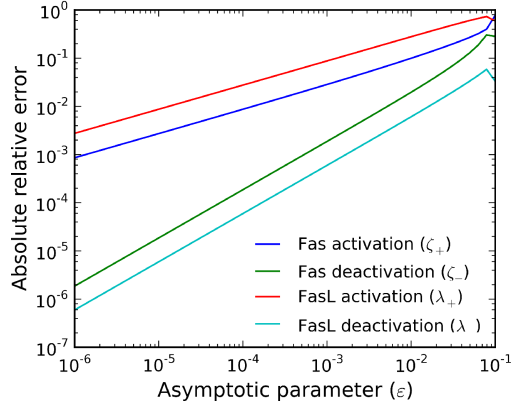
$$p_\lambda(\zeta_-) \sim -\alpha^2\beta\zeta_-^2 - \alpha^2(\alpha\delta - \beta)\zeta_-, \quad q_\lambda(\zeta_-) \sim \alpha^2\gamma\zeta_-^3 - \alpha^2(\gamma - 1)\zeta_-^2 - \alpha^2\zeta_-,$$

so

$$\lambda_- = f_\lambda(\zeta_-) \sim \frac{\beta}{\gamma\Delta + \Theta - 2\sqrt{\gamma\Delta\Theta}}, \quad (8)$$

which, in particular, is positive if $\Theta \geq 0$ as, in this case, the nontrivial positivity condition is

$$\sqrt{\frac{\gamma\Delta}{\Theta}} + \sqrt{\frac{\Theta}{\gamma\Delta}} > 2,$$



Supplementary Figure 1 Relative errors of approximation of the asymptotic forms of the Fas and FasL thresholds ζ_{\pm} and λ_{\pm} , respectively, with respect to the numerically computed thresholds.

which is satisfied since $\Theta = \gamma\Delta - (\gamma + 1) < \gamma\Delta$, so $\gamma\Delta/\Theta \neq 1$. Therefore, all thresholds ζ_{\pm} and λ_{\pm} are real and nonnegative if (6) holds.

We verified the accuracy of the asymptotic forms of ζ_{\pm} and λ_{\pm} by letting

$$\alpha = \frac{5}{\varepsilon}, \quad \beta = 1, \quad \gamma = 5, \quad \delta = \varepsilon$$

(so that the baseline is achieved with $\varepsilon = 10^{-2}$) and comparing with the numerically computed thresholds over $10^{-6} \leq \varepsilon \leq 10^{-1}$. The results confirm the analysis and furthermore reveal that ζ_{+} and λ_{+} have relative approximation errors of $\mathcal{O}(\sqrt{\varepsilon})$; and ζ_{-} and λ_{-} , $\mathcal{O}(\varepsilon)$ (Supplementary Figure 1).

1.2 Threshold variation data statistics

The statistics of the threshold variation data (Dataset 1; $N = 10^3$, $\chi = 0.25$) are observed to match well with expectations and furthermore reveal the effect of total parameter variation on the bistability thresholds λ_{\pm} (Supplementary Table II). Moreover, parameter-threshold correlations suggest that both λ_{\pm} are relatively insensitive to β , with λ_{+} being additionally robust to γ (Supplementary Table III).

1.3 Discrete variation analysis for robustness of bistability

In the main paper, we described data (Dataset 2) that suggested convergence of the bistable fraction to 0.5 as the magnitude of parameter variation $\chi \rightarrow \infty$. This asymptotic value may be explained using a very simple discrete analysis. Characterize the variation of each parameter as either greater or less than the baseline, and assume that all variation is identical in proportion. Propagate changes in α , β , and δ to Δ using (3), and further assume that variation is large so that $\Delta > \Delta^*$ if the net result is an overall increase, and $\Delta < \Delta^*$ if a decrease (Supplementary Table IV); recall that, given $\gamma > 1$, $\Delta > \Delta^*$ is the asymptotic bistability condition, which has been validated against the threshold variation data (Dataset 1). Since the baseline values are also the median values of the parameter distributions, each variation occurs independently with probability 1/2, so each outcome is equally likely. Therefore, assuming that $\gamma > 1$, the bistable fraction (Δ with + variation) is also 1/2.

Supplementary Table II Parameter and threshold statistics for threshold variation data (Dataset 1). The data comprise $N = 10^3$ trials drawn by independently sampling each parameter from a log-normal distribution with a scaled standard deviation of $\chi = 0.25$ about its baseline median value. Bistability thresholds were computed numerically for each parameter set, with statistics computed only over bistable sets.

	Quantity	Maximum	Minimum	Median	Norm. std. dev.
parameters	α	1116.760	225.184	505.387	0.252
	β	2.086	0.453	1.007	0.252
	γ	10.859	1.887	4.989	0.254
	δ	0.023	0.005	0.010	0.250
thresholds	λ_+	11.020	0.636	3.258	0.504
	λ_-	8.297	0.579	2.482	0.480

Supplementary Table III Parameter-threshold correlations for threshold variation data (Dataset 1). Correlations were computed only over bistable parameter sets.

Threshold	Parameter	Correlation
λ_+	α	+0.724982
	β	-0.148639
	γ	-0.168286
	δ	+0.638670
	Δ	+0.855905
λ_-	α	+0.663543
	β	-0.105978
	γ	-0.404652
	δ	+0.620883
	Δ	+0.783721

Supplementary Table IV Discrete variation analysis for robustness of bistability. All variation is independent and assumed binary (+/-, above/below baseline), identical in proportion, and large ($\Delta > \Delta^*$ if +; $\Delta < \Delta^*$ if -). Variations are propagated through $\Delta = \alpha\delta/\beta$, which predicts a 50% bistable fraction, assuming that $\gamma > 1$.

Parameter	Variation							
α	+	+	+	+	-	-	-	-
β	+	+	-	-	+	+	-	-
δ	+	-	+	-	+	-	+	-
Δ	+	-	+	+	-	-	+	-

Supplementary Table V Order balance of $p_\lambda = \sum_{i=0}^2 c_i \zeta_\infty^i$. Top, critical values of ν , where $\zeta_\infty = \mathcal{O}(\varepsilon^\nu)$ for $\varepsilon \ll 1$, balancing each pair of terms in p_λ ; bottom, corresponding ε -exponent of the order of each term. Admissible balances are enclosed in parentheses.

	$c_2 = \mathcal{O}(\varepsilon^{2\nu-2})$	$c_1 = \mathcal{O}(\varepsilon^{\nu-2})$	$c_0 = \mathcal{O}(\varepsilon^{-1})$
c_2	—	0	1/2
c_1		—	1
c_0			—
(1)	0	(-1)	(-1)
1/2	-1	-3/2	-1
(0)	(-2)	(-2)	-1

2 Parameter identification

The values of the thresholds ζ_\pm and λ_\pm may be used to estimate the model parameters in the asymptotic limit (1). To facilitate the estimation, we further require the unique value ζ_0 of ζ_∞ at $\lambda = 0$, which is given by solving $p_\lambda = 0$. Performing an order balance for p_λ as in §1.1, we found that $\nu = 0$ and 1 (Supplementary Table V), so

$$\zeta_0 \sim \begin{cases} 2/[\alpha(\Delta-1)], & \Delta > 1, \\ 1-\Delta, & \Delta \leq 1. \end{cases} \quad (9)$$

As the ζ_\pm and λ_\pm are assumed to exist, we hence defined ζ_0 by the first formula.

We may then solve, for example, ζ_0 , λ_+ , and ζ_+ for α , β , and γ , respectively as functions of Δ , i.e.,

$$\alpha = \frac{2}{(\Delta-1)\zeta_0}, \quad \beta = \frac{\Delta-1}{\lambda_+}, \quad \gamma = \frac{\Delta}{\Delta-1} \left(1 + \frac{2}{\alpha\zeta_+^2} \right), \quad (10)$$

and finally, obtain Δ by simultaneous optimization of both ζ_- and λ_- , subject to the bistability constraint $\Delta > \Delta^*$. The value of δ is recovered through Δ .

To set the nondimensional timescale k_{-1} , we considered the characteristic time for convergence to the steady state. The Jacobian matrix

$$J = \begin{pmatrix} \xi_{\tau\xi} & \xi_{\tau\zeta} \\ \zeta_{\tau\xi} & \zeta_{\tau\zeta} \end{pmatrix} \Big|_\infty$$

evaluated at steady state, i.e., at $\eta = (1 - \zeta_\infty)/(1 + \alpha)$, has the eigenvalues

$$\mu_1 = -1, \quad \mu_2 = -\frac{\delta}{\varepsilon} + \mathcal{O}(\varepsilon), \quad (11)$$

where we assumed $\zeta_\infty, \lambda = \mathcal{O}(1)$ for cell death. Therefore, the nondimensional relaxation time is $\tau_{\text{relax}} = \max\{-1/\mu_{1,2}\} = \mathcal{O}(1)$, so by rescaling, $k_{-1} = \tau_{\text{relax}}/t_{\text{relax}} = \mathcal{O}(1/t_{\text{relax}})$, where t_{relax} is the experimentally measured relaxation time. This leaves only one of $k_l^{(2)}$ and $k_l^{(3)}$ undetermined.

Supplementary Table VI Reaction rates of the stochastic formulation of the hysteron model with $n = 3$ in a reaction area A , where lowercase letters denote the molecule numbers of the corresponding uppercase species.

Reaction	Rate
$Y \rightarrow X$	$k_1 y$
$X \rightarrow Y$	$k_{-1} x$
$2Y \rightarrow 2Z$	$k_2 y(y-1)/A$
$Y + Z \rightarrow 2Z$	$k_2 y z / A$
$Z \rightarrow Y$	$k_3 Z$
$L + X \rightarrow L + Y$	$k_4 l x / A$
$L + 2Y \rightarrow L + 2Z$	$k_l^{(2)} l y (y-1) / A^2$
$L + Y + Z \rightarrow L + 2Z$	$k_l^{(2)} l y z / A^2$
$L + 3Y \rightarrow L + 3Z$	$k_l^{(3)} l y (y-1)(y-2) / A^3$
$L + 2Y + Z \rightarrow L + 3Z$	$k_l^{(3)} l y (y-1) z / A^3$
$L + Y + 2Z \rightarrow L + 3Z$	$k_l^{(3)} l y z (z-1) / A^3$

3 Stochastic simulation

For completeness, we derived also a stochastic formulation of the hysteron model with $n = 3$, with modified reaction rates depending on the reaction area A (Supplementary Table VI). For illustration, we considered a reaction area of $1 \mu\text{m}^2$, roughly $1/600^{\text{th}}$ of that of the cell membrane, corresponding to a total of ~ 10 receptors, assuming a uniform distribution. We assumed the initial condition

$$\#X = 8, \quad \#Y = 0, \quad \#Z = 2, \quad \#L = 1,$$

where number notation denotes molecule number, as an intermediate state that will allow the sampling of both deterministic steady states, and used the Gillespie algorithm (Gillespie, 1977) to generate an ensemble of $N = 20$ trajectories at baseline parameters (Supplementary Table VII). Trajectories visiting both low and high $\#Z$ are obtained (Supplementary Figure 2), notably in contrast to the deterministic model, which allows only convergence to the death state as the corresponding threshold is $\#L \sim 0.1$.

4 Comparison with the crosslinking model

4.1 Solution of crosslinking model

From Box 2, the steady-state FasL-Fas complex concentrations are

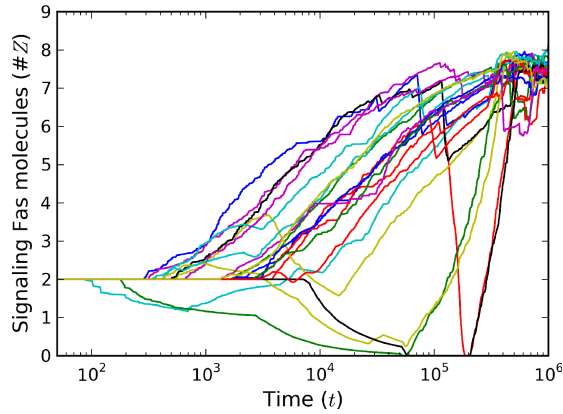
$$\gamma_{1,\infty} = 3\lambda_\infty \left(\frac{\rho_\infty}{\kappa}\right), \quad \gamma_{2,\infty} = 3\lambda_\infty \left(\frac{\rho_\infty}{\kappa}\right)^2, \quad \gamma_{3,\infty} = \lambda_\infty \left(\frac{\rho_\infty}{\kappa}\right)^3, \quad (12)$$

so apply ligand conservation, i.e., $\lambda_0 = \lambda + \gamma_1 + \gamma_2 + \gamma_3$, at steady state to obtain

$$\lambda_\infty = \frac{\lambda_0}{1 + 3(\rho_\infty/\kappa) + 3(\rho_\infty/\kappa)^2 + (\rho_\infty/\kappa)^3}, \quad (13)$$

Supplementary Table VII Baseline dimensional parameter values for the hysteron and caspase models. Parameters were derived from the corresponding nondimensional baseline values assuming $s = 10$ nM, $k_{-1} = 10^{-2} \text{ min}^{-1}$, and $k_l^{(2)} = 10^{-2} \text{ nM}^{-2} \text{ min}^{-1}$ for the hysteron model; and $\Omega = 100$ nM and $k_{-3} = 10^{-3} \text{ min}^{-1}$ for the caspase model. For SBML computations, we set $k_4 = 0.1 \text{ nM/min}$.

Model	Parameter	Value
hysteron	k_1	5 min^{-1}
	k_{-1}	10^{-2} min^{-1}
	k_2	$10^{-3} \text{ nM}^{-1} \text{ min}^{-1}$
	k_3	10^{-4} min^{-1}
	k_4	$0 (0.1) \text{ nM}^{-1} \text{ min}^{-1}$
	$k_l^{(2)}$	$10^{-2} \text{ nM}^{-2} \text{ min}^{-1}$
	$k_l^{(3)}$	$5 \times 10^{-3} \text{ nM}^{-3} \text{ min}^{-1}$
caspase	k_1	$10^{-4} \text{ nM}^{-1} \text{ min}^{-1}$
	k_2	$10^{-4} \text{ nM}^{-1} \text{ min}^{-1}$
	k_3	1 nM/min
	k_{-3}	10^{-3} min^{-1}
	k_4	10^{-3} min^{-1}



Supplementary Figure 2 Stochastic simulation of the hysteron model for an ensemble of $N = 20$ trajectories in a reaction area $A = 1 \mu\text{m}^2$ using baseline parameter values (Supplementary Table VII). Trajectories were smoothed using a moving average with time window $\approx 3 \times 10^5$ min.

where ρ_∞ is given by applying receptor conservation, i.e., $1 = \rho + \gamma_1 + 2\gamma_2 + 3\gamma_3$, and solving

$$\rho_\infty^4 + (3\lambda_0 + 3\kappa - 1)\rho_\infty^3 + 3\kappa(2\lambda_0 + \kappa - 1)\rho_\infty^2 + \kappa^2(3\lambda_0 + \kappa - 3)\rho - \kappa^3 = 0,$$

which has the unique nonnegative root

$$\rho_\infty = \frac{1}{2} \left[\sqrt{(3\lambda_0 + \kappa - 1)^2 + 4\kappa} - (3\lambda_0 + \kappa - 1) \right]. \quad (14)$$

4.2 Steady-state invariants

Steady-state invariants (Box 3) for the hysteron and crosslinking models were computed as outlined in the Materials and methods using Sage (<http://www.sagemath.org/>), giving

$$\omega_H(\lambda_0, \zeta) = c_{13}\lambda_0\zeta^3 + c_{12}\lambda_0\zeta^2 + c_{11}\lambda_0\zeta + c_{02}\zeta^2 + c_{10}\lambda_0 + c_{01}\zeta + c_{00}, \quad (15)$$

where

$$\begin{aligned} c_{13} &= -\alpha^2\gamma - 2\gamma, \\ c_{12} &= \alpha^2(\gamma - 1) - 2\alpha\gamma + 6\gamma + 1, \\ c_{11} &= \alpha^2 + 2\alpha(\gamma - 1) - (7\gamma + 3) \\ c_{02} &= -\alpha^2\beta + \beta, \\ c_{10} &= 2\alpha + 3\gamma + 2, \\ c_{01} &= -\alpha^2(\alpha\delta - \beta) - \alpha(3\alpha\delta + 2\beta) - 3(\alpha\delta + \beta) - \delta, \\ c_{00} &= 2\alpha\beta + 2\beta, \end{aligned}$$

and

$$\omega_C(\lambda_0, \zeta) = 3\lambda_0\zeta - \zeta^2 - 3\lambda_0 + (\kappa + 1)\zeta, \quad (16)$$

respectively. Correctness of ω_H may be shown by observing that $\omega_H/\zeta_\tau = (\alpha + 1)^3$ is constant under the identification $\lambda = \lambda_0$; similarly, we demonstrate correctness of ω_C by verifying that $\omega_C = 0$ for $\zeta = \gamma_{1,\infty} + 2\gamma_{2,\infty} + 3\gamma_{3,\infty}$.

4.3 Nonnegative least squares for model discrimination

To cast the optimization of ω_H and ω_C into nonnegative least squares (NNLS) form, we linearized the problem by considering ω_H and ω_C as functions of

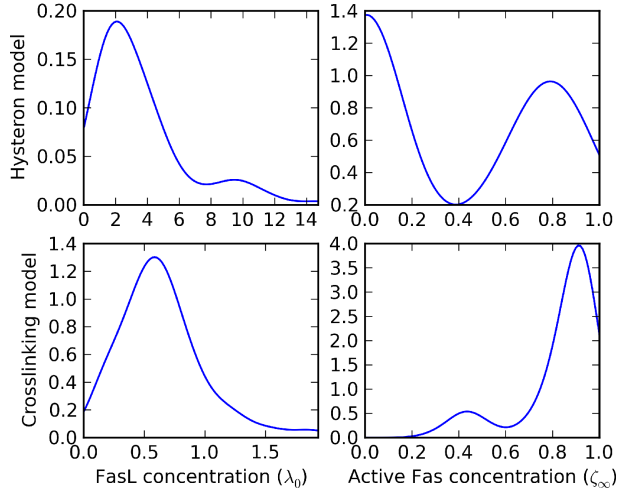
$$\mathbf{x}_H = (-\lambda_0\zeta^3, \lambda_0\zeta^2, \lambda_0\zeta, -\zeta^2, \lambda_0, -\zeta, 1), \quad \mathbf{x}_C = \zeta,$$

respectively. Then, given experimental data $U = (\lambda_0, \zeta_\infty)$, we may write

$$\omega(U; c) = Uc(\mathbf{a}) - b(U), \quad (17)$$

suppressing model reference for generality, where U is a row vector corresponding to the data represented in terms of the variables \mathbf{x} ; $c(\mathbf{a})$ is a column vector of nonnegative coefficients in the model parameters \mathbf{a} to be determined, constrained by the limit (1) with $\Delta > 1$; and b is a column vector of constants given the data. For the hysteron model,

$$c_H \in \mathbb{R}_+^7, \quad b_H = -\lambda_0\zeta^2 + 3\lambda_0\zeta - 2\lambda_0,$$



Supplementary Figure 3 Distributions of the invariant measurables λ_0 , the total FasL concentration, and ζ_∞ , the steady-state active Fas concentration, for data generated from the hysteron and crosslinking models (Datasets 3 and 4).

where we have used subscript notation in the obvious manner and \mathbb{R}_+ denotes the nonnegative real numbers, while for the crosslinking model,

$$c_C \in \mathbb{R}_+, \quad b_C = -3\lambda_0\zeta + \zeta^2 + 3\lambda_0 - \zeta.$$

For many experimental trials, U is considered instead a matrix, with each row denoting an individual sample, so that $\omega(U; c) = 0$ now gives an overdetermined system. This leads to a natural least squares problem for $\epsilon = \|\omega\| = \|Uc - b\|$ as a function of c , which in particular is in NNLS form given the nonnegativity of c . A significant advantage of NNLS over direct nonlinear optimization is that ϵ is minimized exactly, producing an error that is indeed a global minimum (Lawson and Hanson, 1995).

4.4 Performance of model discrimination

As described in the main paper, we tested the NNLS formulation for model discrimination, using $N = 100$ samples generated from each model (Datasets 3 and 4), chosen based on the dimensions of c_H and c_C . The results show that errors are low if the models underlying the data generation and the invariant minimization are the same, and large otherwise. Note that NNLS provides a lower bound to the cross-model errors due to the introduction of additional degrees of freedom for linearization. Furthermore, we remark that the crosslinking-crosslinking optimization was able to recover the coefficient $\kappa + 1$ of ζ in ω_C to machine precision.

To verify that these results should hold generally, we analyzed the distributions of the data λ_0 and ζ_∞ (Supplementary Figure 3). The data are clearly nondegenerate, so we expect that the results are representative.

Supplementary Table VIII Initial concentrations for the SBML implementations of the hysteron and hysteron-caspase models. For sensitivity analyses, the FasL (L) concentration was set to $l = 0.1$ nM (within the bistable regime). FasL is considered a species only nominally and is otherwise treated as a parameter.

Model	Species	Initial condition (nM)
hysteron	X	10
	Y	0
	Z	0
	L	0.2 (0.1)
caspase	Casp8	100
	Casp8*	0
	Casp3	100
	Casp3*	0

5 SBML implementation

5.1 Model definition

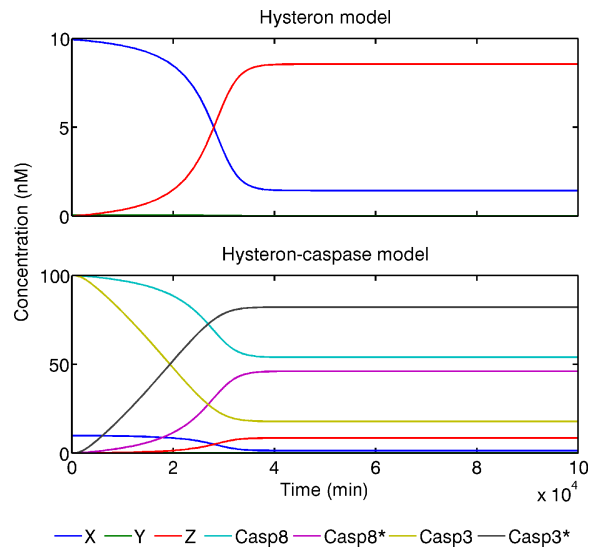
The hysteron and hysteron-caspase models with $n = 3$ were implemented in dimensional form using the Systems Biology Markup Language (SBML) Level 2 Version 1 (Finney and Hucka, 2003; Hucka et al., 2003) and are named `hysteron.xml` and `hysteron-caspase.xml`, respectively. Corresponding dimensional baseline parameters were used, though we did not restrict $k_4 = 0$ ($\theta = 0$) as in the nondimensional case (Supplementary Table VII). Initial concentrations (Supplementary Table VIII) were estimated from the literature (Albeck et al., 2008a,b; Bagci et al., 2006; Bentele et al., 2004; Eißing et al., 2004; Harrington et al., 2008; Hua et al., 2005; Legewie et al., 2006; Okazaki et al., 2008; Rangamani and Sirovich, 2007), though we caution that substantial variation exists (see Svingen et al., 2004). Time course simulation of the models validates their definition (Supplementary Figure 4).

We demonstrate the SBML models below by using standard SBML-compliant software (see Bergmann and Sauro, 2006).

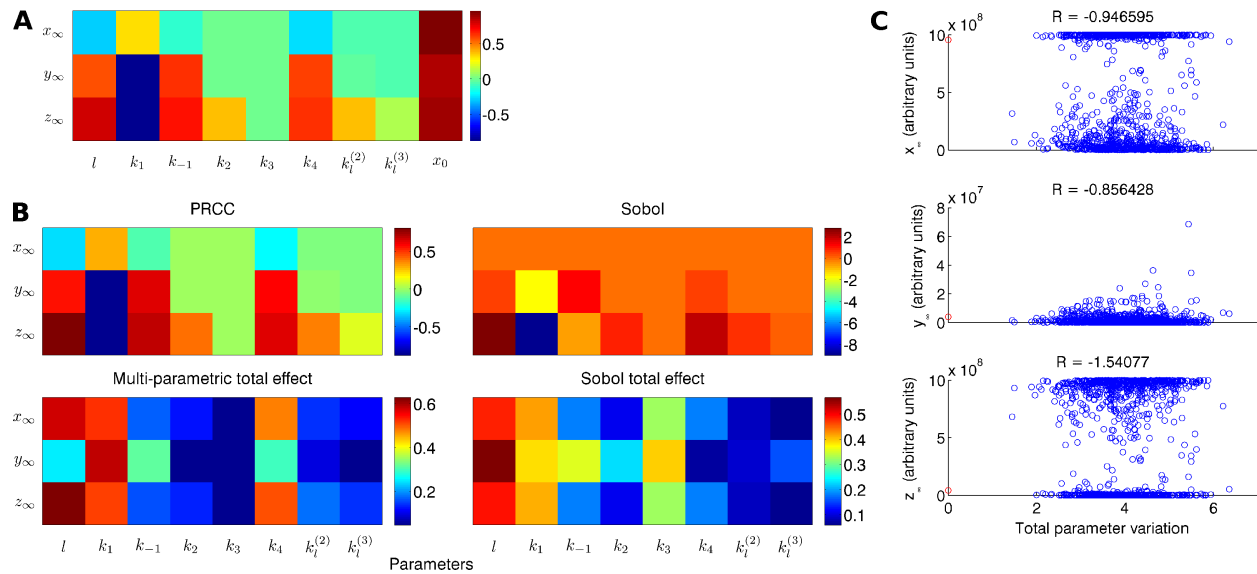
5.2 Sensitivity analysis

Sensitivity analysis of the hysteron model was performed with respect to the steady state by using openly available toolboxes such as SBML-SAT (Zi et al., 2008) and SBTOOLBOX2 (Schmidt and Jirstrand, 2006). Local sensitivity analysis was conducted using SBML-SAT with a perturbation coefficient of 0.01 about baseline parameters (Supplementary Tables VII and VIII). The results highlight the importance of the parameters l , the FasL concentration; $k_{\pm 1}$, the rates of constitutive receptor closing and opening, respectively; k_4 , the rate of ligand-induced receptor opening; and x_0 , the initial Fas concentration (Supplementary Figure 5A). These corroborate, but do not completely reproduce, the nondimensional analysis.

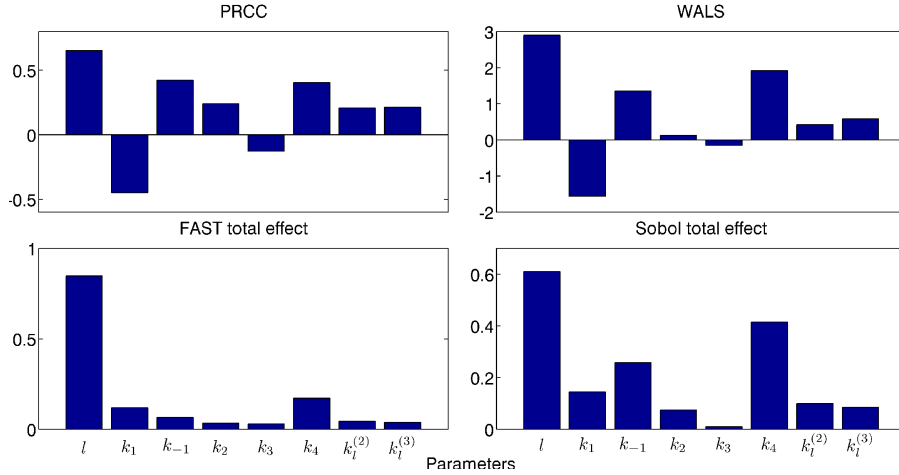
We also performed global sensitivity analyses. Methods employed include partial rank correlation coefficient analysis (PRCC), Sobol’s method, multi-parametric sensitivity analysis (MPSA), weighted average of local sensitivities (WALS), and the Fourier amplitude sensitivity test (FAST). Briefly, PRCC is based on multiple linear regression, Sobol and FAST are variance-decomposition methods, MPSA uses a classifier-based discrimination scheme, and WALS extends local sensitivity analysis; for details, see Bentele et al. (2004); Chan et al. (1997); Marino et al. (2008); Saltelli et al. (2005); Sobol’ (2001); Turányi (1990); Zheng



Supplementary Figure 4 Time courses of SBML hysteron and hysteron-caspase models at baseline parameters and initial conditions (Supplementary Tables VII and VIII).



Supplementary Figure 5 Sensitivity and robustness analysis of the hysteron model with respect to the steady state using SBML-SAT. Baseline values as reference (Supplementary Tables VII and VIII). (A) Local sensitivity analysis using a perturbation coefficient of 0.01. (B) Global sensitivity analysis using partial correlation coefficient analysis (PRCC), Sobol's method, and multi-parametric sensitivity analysis. Parameters were perturbed over five orders of magnitude ($N = 2 \times 10^3$ simulations). (C) Robustness analysis using $N = 10^3$ perturbations.



Supplementary Figure 6 Global sensitivity analysis of the hysteron model with respect to the steady state using SBTOOLBOX2. Baseline values as reference (Supplementary Tables VII and VIII). Parameters were perturbed over five orders of magnitude ($N = 2 \times 10^3$ simulations for PRCC, FAST, and Sobol; $N = 10^3$ for WALs).

and Rundell (2006); Zi et al. (2005). Total effect sensitivities account for combinatorial parameter effects. Analyses performed using both SBML-SAT and SBTOOLBOX2 exhibit general consistency in emphasizing the parameters l , $k_{\pm 1}$, and k_4 (Supplementary Figures 5B and 6).

5.3 Robustness analysis

Robustness analysis was also conducted using SBML-SAT. The robustness is defined as

$$R = -\frac{1}{N} \sum_{i=1}^N \left| \log_{10} \left(\frac{\tilde{f}_i}{f} \right) \right|, \quad (18)$$

where f is the reference model output, \tilde{f}_i is the perturbed model output of parameter set i , and N is the number of randomly generated parameter sets (see Kitano, 2007). Note that $R \leq 0$; the closer that R is to zero, the more robust the system. Parameter generation was done using Latin hypercube sampling, with each parameter set characterized by the total parameter variation

$$\text{TPV} = \sum_{i=1}^M \left| \log_{10} \left(\frac{\tilde{k}_i}{k_i} \right) \right|, \quad (19)$$

where k_i and \tilde{k}_i are the reference and perturbed values of parameter i , and M is the number of model parameters. For details, see Barkai and Leibler (1997); Blüthgen and Herzog (2003); Zi and Sun (2005). Results exhibit a double-banded structure for the steady-state concentrations x_∞ and z_∞ , demonstrating robustness in the context of bistability (Supplementary Figure 5C).

6 Datasets

Threshold variation (Dataset 1), bistability robustness (Dataset 2), and hysteron and crosslinking model discrimination (Datasets 3 and 4) data are consolidated in space-delimited format (Supplementary Table IX),

Supplementary Table IX Space-delimited format for stored data. Dataset 1, threshold variation; dataset 2, bistability robustness; dataset 3, hysteron model discrimination; dataset 4, crosslinking model discrimination. Notation as in main text; ¹bistable (true/false), and ²bistable fraction.

Dataset	Column						
	1	2	3	4	5	6	7
1	α	β	γ	δ	λ_+	λ_-	¹ b
2	χ	² b.f.					
3	λ^0	ξ^0	η^0	ζ^0	λ_0	ζ_∞	
4	λ^0	ρ^0	γ_1^0	γ_2^0	γ_3^0	λ_0	ζ_∞

and are named `threshold-variation.txt`, `bistability-robustness.txt`, `hysteron-discrimination.txt`, and `crosslinking-discrimination.txt`, respectively.

References

- Albeck JG, Burke JM, Aldridge BB, Zhang M, Lauffenburger DA, Sorger PK (2008a) Quantitative analysis of pathways controlling extrinsic apoptosis in single cells. *Mol Cell* **30**: 11–25
- Albeck JG, Burke JM, Spencer SL, Lauffenburger DA, Sorger PK (2008b) Modeling a snap-action, variable-delay switch controlling extrinsic cell death. *PLoS Biol* **6**: e299
- Bagci EZ, Vodovotz Y, Billiar TR, Ermentrout GB, Bahar I (2006) Bistability in apoptosis: Roles of Bax, Bcl-2, and mitochondrial permeability transition pores. *Biophys J* **90**: 1546–1559
- Barkai N, Leibler S (1997) Robustness in simple biochemical networks. *Nature* **387**: 913–917
- Bentele M, Lavrik I, Ulrich M, Stößer S, Heermann D, Kalthoff H, Krammer P, Eils R (2004) Mathematical modeling reveals threshold mechanism in CD95-induced apoptosis. *J Cell Biol* **166**: 839–851
- Bergmann FT, Sauro HM (2006) SBW - a modular framework for systems biology. In Perrone LF, Wieland FP, Liu J, Lawson BG, Nicol DM, Fujimoto RM (eds.) *Proceedings of the 2006 Winter Simulation Conference*, pp. 1637–1645. Winter Simulation Conference
- Blüthgen N, Herzog H (2003) How robust are switches in intracellular signaling cascades? *J Theor Biol* **225**: 293–300
- Chan K, Saltelli A, Tarantola S (1997) Sensitivity analysis of model output: variance-based methods make the difference. In Andradóttir S, Healy KJ, Withers DH, Nelson BL (eds.) *Proceedings of the 1997 Winter Simulation Conference*, pp. 261–268. IEEE Computer Society, Washington, DC, USA
- Eißing T, Conzelmann H, Gilles ED, Allgöwer F, Bullinger E, Scheurich P (2004) Bistability analyses of a caspase activation model for receptor-induced apoptosis. *J Biol Chem* **279**: 36892–36897
- Finney A, Hucka M (2003) Systems biology markup language: Level 2 and beyond. *Biochem Soc Trans* **31**: 1472–1473
- Gillespie DT (1977) Exact stochastic simulation of coupled chemical reactions. *J Phys Chem* **81**: 2340–2361

- Harrington HA, Ho KL, Ghosh S, Tung K (2008) Construction and analysis of a modular model of caspase activation in apoptosis. *Theor Biol Med Model* **5**: 26
- Hua F, Cornejo MG, Cardone MH, Stokes CL, Lauffenburger DA (2005) Effects of Bcl-2 levels on Fas signaling-induced caspase-3 activation: Molecular genetic tests of computational model predictions. *J Immunol* **175**: 985–995
- Hucka M, Finney A, Sauro HM, Bolouri H, Doyle JC, Kitano H, Arkin AP, Bornstein BJ, Bray D, Cornish-Bowden A, Cueller AA, Dronov S, Gilles ED, Ginkel M, Gor V, Goryanin II, Hedley WJ, Hodgman TC, Hofmeyr JH, Hunter PJ, et al. (2003) The systems biology markup language (SBML): a medium for representation and exchange of biochemical network models. *Bioinformatics* **19**: 524–531
- Kitano H (2007) Towards a theory of biological robustness. *Mol Syst Biol* **3**: 137
- Lawson CL, Hanson RJ (1995) *Solving Least Squares Problems*. Society for Industrial and Applied Mathematics, Philadelphia, PA, USA
- Legewie S, Blüthgen N, Herzog H (2006) Mathematical modeling identifies inhibitors of apoptosis as mediators of positive feedback and bistability. *PLoS Comput Biol* **2**: e120
- Marino S, Hogue IB, Ray CJ, Kirschner DE (2008) A methodology for performing global uncertainty and sensitivity analysis in systems biology. *J Theor Biol* **254**: 178–196
- Okazaki N, Asano R, Kinoshita T, Chuman H (2008) Simple computational models of type I/type II cells in Fas signaling-induced apoptosis. *J Theor Biol* **250**: 621–633
- Rangamani P, Sirovich L (2007) Survival and apoptotic pathways initiated by TNF- α : Modeling and predictions. *Biotechnol Bioeng* **97**: 1216–1229
- Saltelli A, Ratto M, Tarantola S, Campolongo F (2005) Sensitivity analysis for chemical models. *Chem Rev* **105**: 2811–2828
- Schmidt H, Jirstrand M (2006) Systems Biology Toolbox for MATLAB: a computational platform for research in systems biology. *Bioinformatics* **22**
- Sobol' IM (2001) Global sensitivity indices for nonlinear mathematical models and their Monte Carlo estimates. *Math Comput Simul* **55**: 271–280
- Svingen PA, Loegering D, Rodriguez J, Meng XW, Mesner PWJ, Holbeck S, Monks A, Krajewski S, Scudiero DA, Sausville EA, Reed JC, Lazebnik YA, Kaufmann SH (2004) Components of the cell death machine and drug sensitivity of the National Cancer Institute cell line panel. *Clin Cancer Res* **10**: 6807–6820
- Turányi T (1990) Sensitivity analysis of complex kinetic systems. tools and applications. *J Math Chem* **5**: 203–248
- Zheng Y, Rundell A (2006) Comparative study of parameter sensitivity analyses of the TCR-activated Erk-MAPK signalling pathway. *IEE Proc Syst Biol* **153**: 201–211
- Zi Z, Cho KH, Sung MH, Xia X, Zheng J, Sun Z (2005) In silico identification of the key components and steps in IFN- γ induced JAK-STAT signaling pathway. *FEBS Lett* **579**: 1101–1108
- Zi Z, Sun ZR (2005) Robustness analysis of the IFN- γ induced JAK-STAT signaling pathway. *J Comput Sci Technol* **20**: 491–495
- Zi Z, Zheng Y, Rundell AE, Klipp E (2008) SBML-SAT: a systems biology markup language (SBML) based sensitivity analysis tool. *BMC Bioinformatics* **9**: 342